Biomicrofluidics REVIEW scitation.org/journal/bmf

Liver-on-a-chip: Considerations, advances, and beyond

Cite as: Biomicrofluidics 16, 061502 (2022); doi: 10.1063/5.0106855
Submitted: 30 June 2022 · Accepted: 25 October 2022 ·
Published Online: 8 November 2022

Zhenxu Yang,[1,2,3] Xiaochen Liu,[1,2,3] Elise M. Cribbin,[4] Alice M. Kim,[4] Jiao Jiao Li,[1,4,a)] and Ken-Tye Yong[1,2,3,a)]

AFFILIATIONS

[1]School of Biomedical Engineering, The University of Sydney, Sydney, New South Wales 2006, Australia
[2]The University of Sydney Nano Institute, The University of Sydney, Sydney, New South Wales 2006, Australia
[3]The Biophotonics and Mechanobioengineering Laboratory, The University of Sydney, Sydney, New South Wales 2006, Australia
[4]School of Biomedical Engineering, University of Technology Sydney, New South Wales 2007, Australia

[a)]**Authors to whom correspondence should be addressed:** ken.yong@sydney.edu.au and jiaojiao.li@uts.edu.au

ABSTRACT

The liver is the largest internal organ in the human body with largest mass of glandular tissue. Modeling the liver has been challenging due to its variety of major functions, including processing nutrients and vitamins, detoxification, and regulating body metabolism. The intrinsic shortfalls of conventional two-dimensional (2D) cell culture methods for studying pharmacokinetics in parenchymal cells (hepatocytes) have contributed to suboptimal outcomes in clinical trials and drug development. This prompts the development of highly automated, biomimetic liver-on-a-chip (LOC) devices to simulate native liver structure and function, with the aid of recent progress in microfluidics. LOC offers a cost-effective and accurate model for pharmacokinetics, pharmacodynamics, and toxicity studies. This review provides a critical update on recent developments in designing LOCs and fabrication strategies. We highlight biomimetic design approaches for LOCs, including mimicking liver structure and function, and their diverse applications in areas such as drug screening, toxicity assessment, and real-time biosensing. We capture the newest ideas in the field to advance the field of LOCs and address current challenges.

I. INTRODUCTION

The ability to simulate human physiology outside of the body is invaluable in medical research, enabling the study of disease mechanisms and drug development. The traditional practice is to use a conventional two-dimensional (2D) cell culturing system (i.e., cells in a Petri dish). 2D culture only permits cells to grow in a flat monolayer[1] but has, nevertheless, become an essential platform for studying cellular mechanisms and interactions due to its simplicity and ease of operation.[2] Despite their higher controllability and reproducibility, 2D cultures have much lower physiological relevance and complexity compared to three-dimensional (3D) cultures, as shown in Fig. 1.[3–5]

Conventional cell culturing methods and organ-on-a-chip (OOC) are both considered *in vitro* models.[1–6] A comprehensive analysis between 2D and 3D cultures is presented in Table I. 2D cultured cells experience nutrient depletion over time since there is no fluid flow.[3] Replenishment of cell culture medium is required for the continuous growth of cells. In addition, 2D cell culture often only permits the study of a single cell type. Compared to the native *in vivo* environment where cells are normally located, 2D cell cultures on a flat surface pose a clear disadvantage. In comparison, 3D culturing and OOC can encourage cell–cell communications and produce physiologically relevant data.[3–8] OOC is a microfluidic-based platform that bridges between 2D cell culture and animal models, mimicking the critical aspects of human physiology. Since the development of the first mechanically actuatable lung-on-a-chip device in 2010,[9] there has been a plethora of work on OOC for different organs, such as the intestine,[10,11] brain,[12,13] blood–brain-barrier,[14,15] and multi-organ system.[16,17]

In this review, we will focus on liver-on-a-chip (LOC), which is a sub-group of OOC. LOC has attracted increasing attention over the years, with recent developments aimed at recapitulating the *in vivo* tissue structure, functions, biochemical cues, and microenvironment of the liver, which conventional 2D culturing has failed to

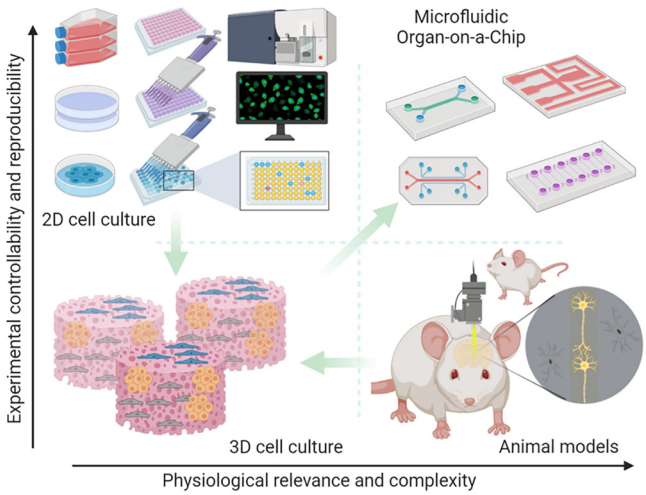

FIG. 1. Preclinical studies rely on major tools, including 2D or 3D *in vitro* cell cultures, and *in vivo* animal models, for drug development. 2D culture offers a rapid and reproducible way to analyze drug response; however, they lack the 3D physiological tissue environment. Conventional 3D culture can provide a 3D environment but still falls short of controllably recapitulating the *in vivo* physiology and pathology of the human body. Animal models enable *in vivo* analysis, yet the species differences between animal and human physiological mechanisms and the complexity of *in vivo* physiology weakens the accuracy and reproducibility of experimental results. A microfluidic organ-on-a-chip platform that enables controllable cell culture within an organotypic microarchitectural environment provides a simple yet more physiologically relevant platform to controllably and systematically interrogate human biology. Figure generated in BioRender (BioRender.com). Reproduced with permission from Ma *et al.*, Trends Pharmacol. Sci. **42**(2), 119–133 (2021). Copyright 2021 Elsevier Ltd.

achieve.[6–18] lOC allows the study of drug metabolism in models relevant to human physiology and offers an alternative approach to animal models.[19,20] Although animal studies are still required during drug development to assess drug efficacy and toxicity before human trials, increasing evidence has suggested that animal models may not sufficiently reflect human physiological conditions, and numerous failed trials are becoming an increasing source of concern.[21–23] lOC can be a solution that minimizes ethical hurdles while producing accurate and high throughput scientific data, especially in the context of drug toxicity predictions.[23–27] Besides drug development, nanomedicine toxicity assessment can also be a rising application of LOC.[28–32] With mRNA vaccines and lipid-based nanotechnology for vaccine manufacture, nanomedicine has been brought to the public on an unprecedented scale.[33] However, the lack of policies and protocols for nanotoxicity evaluation has raised concerns.[32] With a handful of Food and Drug Administration (FDA) approved nanomedicine solutions available on the market, it is time to rethink methods that could safely bring nanomedicine into critical care.[34] lOC could find application in the assessment of nanomaterials and other drugs in the context of treatment-induced liver injuries.[35,36]

We will critically discuss these applications and provide fresh insights into the future of LOCs. We will highlight the recent developments in designing LOCs and fabrication strategies, with a focus on the various approaches to achieve a biomimetic design of LOCs. Furthermore, our review critically highlights the gap in evaluating nanomedicine toxicity, and how LOCs can be used to address these gaps. Finally, we conclude with a forward look into the challenges and novel aspects of the advancement of LOCs. We hope to provide fresh perspectives and new application ideas for the next generation LOCs, particularly modeling-based work, such as pharmacometrics, fluid dynamics, and machine learning-aided designs, which supplements a number of recent reviews on different aspects of LOC technology.[26–39]

II. DEVELOPMENT OF LIVER-ON-A-CHIP (LOC) SYSTEMS

Cell–cell and cell–extracellular interactions are critical factors in influencing cellular behavior.[40,41] 2D cell cultures do not allow many of these interactions and are often ineffective in predicting physiologically relevant drug efficacy and toxicity profile. This eventually may lead to failure in drug validation and approval processes for clinical application.[42] Thus, it is essential to recognize that although 2D cell culturing could offer greater flexibility and has been a pivotal part of modern scientific advances, state-of-the-art technologies such as 3D cultures, and OOC platforms are more physiologically relevant evaluation strategies.[3] To overcome the drawbacks of conventional culturing methods, efforts have been made to engineer OOCs that consider the spatial organization of cells.[40–45]

A. *In vitro* cell study methods

Cells in their native environment are intrinsically surrounded by other cells in an interconnected 3D matrix. 2D cell culture fails to address the complex spatial, biochemical, and mechanical requirements of *in vivo* architecture and microenvironments.[46] There is growing evidence that 3D-cultured cells can better recapitulate or even completely resemble *in vivo* cellular responses. One of the advantages of 3D culture is the ability to recapitulate the native tissue environment.[2–43] Such systems permit the study of cell responses to mechanical cues, cell–cell interactions, and extracellular matrix (ECM) communication. Unlike 2D monolayer adherent cell culture, 3D cell culture takes into account the spatial organization of cellular structures.[43] This is an extra dimension compared to 2D culture that significantly impacts molecular signal transduction, allowing physiologically relevant gene expression, morphological changes, and even directing stem cell lineage *in vitro*.

Over the last decades, different *in vitro* models have been developed to simulate liver physiology. One of these techniques is to produce 3D spheroids. Spheroids are "multicellular spherical structures composed of aggregated cells that do not adhere to a substrate but adhere to each other."[47] Primary human hepatocytes (PHH) can give invaluable information for studies on cell metabolism, inflammation, preclinical drug screening, toxicology screenings, and the development of bioartificial liver devices.[48] Despite the view of PHH as a gold-standard cellular model, its drawbacks include a short lifetime during *in vitro* culture, rapid loss of liver-specific function and morphology, the tendency to undergo fibrosis, and weak proliferation capabilities.[49,50] It has been shown that cultivation of PHH in 3D spheroids can more closely recapitulate human liver function. The main advantage of such methods is the ability to retain cell–cell contacts, cell viability, and mature hepatic phenotypes.[51]

TABLE I. Comparison between conventional two-dimensional cell culturing technique and three-dimensional cell culturing technique.[1–76]

Parameters	Two-dimensional	Three-dimensional	
	Monolayer Petri dish culture	Liver organoids	Liver-on-a-chip
General characteristics	Cells grow on rigid tissue culture plastic in monolayer fashion	Usually cultured with hydrogel or as suspension culture where the cell mass is clustered	Gas permeable polymeric membrane usually used as culturing chamber material where cells are encouraged to reconstruct extracellular matrix (ECM); multicellular interactions can be easily encouraged
Cell morphologies	Unnatural cell spreading, limited ECM secretion and limited cell–cell interaction	Possess similar hepatic physiological architecture and excellent cell–cell and ECM interactions	Can achieve close resemblance of physiological and pathological hepatic architecture, high level of ECM production and cell–cell/cell–surface interactions
Flow characteristics	Cannot induce flow parameters; regular replenishing of culture media is required	Can induce flow depending on the design of the bioreactor	Controllable flow parameters, such as shear stress and recirculation of metabolites
Signaling molecules and mass transfer	Short range	Due to formation of spheroids, inner cell mass experience limited mass transfer which could result in cell apoptosis	Accurate control of signaling molecules and nutrients spatially and over time. Incorporations of non-parenchymal cells can more accurately mimic physiological conditions and produce clinically relevant data
High throughput screening (HTS)	A widespread model for HTS	Depending on the platforms used, the throughput levels may vary	Depending on the designed platform, it could be achieved but is limited by the technical challenges
Experimental data	Ease of operation but single time-point data	Difficult to obtain homogenous data	Able to perform real-time monitoring of metabolites over the entire course of the experiment

In recent studies, the emergence of spheroids and commercially available spheroid culture plates has led to their use in OOC. The combination of OOC and liver spheroids have shown great promise in recapitulating liver physiology,[52–54] liver pathology,[47–55] liver xenobiotic/drug metabolism,[6–56] and liver regeneration mechanism.[57] To properly define LOC, there are three characteristic requirements: (1) 3D cell culturing environment;[58] (2) the integration of multiple cell types;[27–59] and (3) the presence of biochemical and biomechanical forces that are native to the designed organ or tissue.[41–60] OOC systems allows precise, systematic control (intensity, duration, and pattern) and cyclic strains on a cell culture substrate to mimic the mechanical forces a cell may experience in its native environment.[61] These platforms can be beneficial for studying mechanotransduction, where modular control of different types of mechanical forces is critical to understanding cellular behavior.[62–64] To create a native niche for liver cells, there are several non-parenchymal cells (non-hepatocytes) that perform critical functions, which should be included with *in vitro* cultures of hepatocytes. Many multi-cellular or co-culturing systems have been developed to recreate such organic interactions between different cell types to promote cross-talk of cytokines and signaling molecules.

B. A brief history of LOCs

The first LOC was reported in 2007 by Philip Lee *et al.*, 3 years before the first lung-on-a-chip.[52] Much attention was given to Huh *et al.* due to the novel introduction of tunable mechanical forces in the lung-on-a-chip design, mimicking human breathing patterns.[9] The introduction of mechanical forces was not incorporated in early LOC devices due to the static nature of the liver. Following this, further understanding of mechanotransduction in cell development and function has broadened the definition of mechanical forces from macroscopic stretching to microscopic shearing forces.[62] Recent LOCs have paid greater attention to such aspects, making them an intricate and desired platform for pathophysiological, mechanistic, and drug toxicity studies. Typical LOC devices contain the parenchymal cells (hepatocytes) as the main or sole cell type. It is now generally recognized by the scientific community that monocellular culturing of hepatocytes does not accurately reflect physiological conditions[2–4] or produce accurate results compared to *in vivo* models.[3] In recent advancements of LOCs, many have incorporated multicellular culturing or co-culturing to better recapitulate the physiological state of the human liver.[25–67]

As shown in Fig. 2, LOC designs have advanced from the simplistic monocellular single-channel device model to a multiple-chip multi-cellular system for studying anticancer drug metabolism effects. In 1998, the introduction of poly(dimethylsiloxane) (PDMS) as an elastomer for rapid prototyping accelerated the field of LOCs and OOCs in general.[68] In 2007, Lee *et al.* published their design of LOC to encourage biliary formation using a perfusion-based system.[52] Then, Nakao *et al.* took Lee's model further to

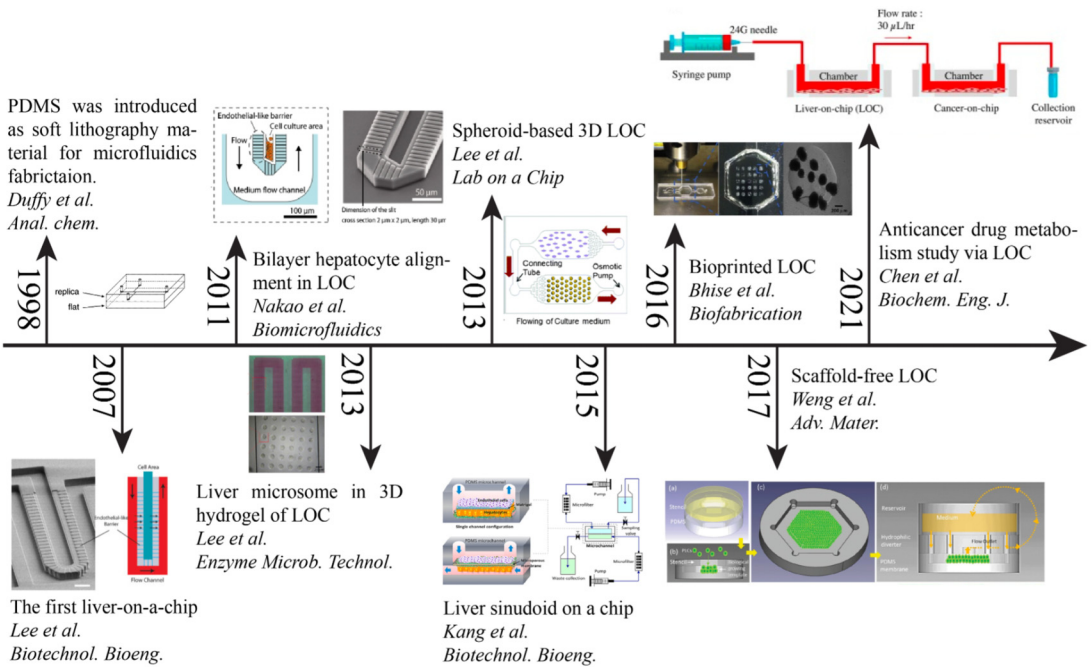

FIG. 2. Timeline of the development of microfluidics-based liver-on-a-chip (LOC) technology. Evolution of the field from the early concept of endothelial barrier-like micropillar by Lee *et al.* in 2007 to the more complex multi-purpose LOC for drug efficacy study reported by Chen *et al.* in 2021. Reproduced with permission from [Copyright permissions: 1998—Reproduced with permission from Duff *et al.*, Anal. Chem. **70**(23), 4974–4984 (1998). Copyright 1998, American Chemical Society. 2007—Reproduced with permission from Lee *et al.*, Biotechnol. Bioeng. **97**(5), 1340–1346 (2007). Copyright 2007 Wiley Periodicals, Inc. 2011—Reproduced with permission from Nakao *et al.*, Biomicrofluidics **5**(2), 022212 (2011). Copyright 2011 AIP Publishing LLC. 2013—Reproduced with permission from Lee *et al.*, Enzyme Microb. Technol. **53**(3), 159–164 (2013). Copyright 2013 Elsevier Inc. 2013—Reproduced with permission from Lee *et al.*, Lab Chip **13**(18), 3529–3537 (2013).Copyright 2013 the Royal Society of Chemistry. 2015—Reproduced with permission from Kang *et al.*, Biotechnol. Bioeng. **112**(12), 2571–2582 (2015). Copyright 2015 Wiley Periodicals, Inc. 2016—Reproduced with permission from Bhise *et al.*, Biofabrication **8**(1), 014101 (2016). Copyright 2016 IOP Publishing Ltd. 2017—Reproduced with permission from Weng *et al.*, Adv. Mater. **29**(36), 1701545 (2017). Copyright 2017 John Wiley & Sons. 2021—Reproduced with permission from Chen *et al.*, Biochem. Eng. J. **165**, 107831 (2021). Copyright 2021 Elsevier B.V.].

precisely control the number of cells allowed in the channel by modifying the design into asymmetric patterns.[69] Nakao *et al.* restricted two-line cell seeding in the channel and promoted biliary formation. Since numerous studies have suggested that 3D scaffolding affects cellular responses, a 3D hydrogel was designed to study the interactions between liver microsomes and hepatocytes by Lee *et al.*[70] They utilized polyethyleneglycol (PEG) pillars within a weaving channel and rat liver microsomes enclosed in a 3D hydrogel matrix. Seven different substrates were tested for the P450 reaction in a microsome solution, creating a metabolic liver model. In the same year, another group showed that a continuous supply of oxygen and nutrients, and removal of wastes using an osmotic pump could assist the long-term maintenance of hepatocyte spheroids.[71] Kang *et al.* in 2015 co-cultured hepatocytes with endothelial cells, and demonstrated long-term maintenance of normal cellular morphology and urea production for up to 30 days.[72] A direct-write bioprinter was used to create the bioreactor by Bhise *et al.* in 2016.[73] The tissue-like construct was assessed over 4 weeks in conjunction with the cellular response of acute acetaminophen (APAP) exposure for predicting drug toxicity. Rather than making direct interaction with the substrate, a scaffold-free technique that encouraged the formation of organoids was demonstrated by Weng *et al.* in 2017.[74] This design took inspiration from liver anatomy where the portal inlets flow radially into the hepatic central outlet, mimicking the structure of liver lobules. It was found that this biomimicry design approach achieved the reconstruction of hepatic cord-like architecture and the formation of fenestrated window-like nanostructures after 7 days of incubation. Recent efforts have been dedicated to drug metabolism screening with multi-chip systems, such as the work by Chen *et al.* in 2021.[75] The LOC was combined with a cancer-on-a-chip (PC3, HepG2, A549, and MCF-7) system to study the liver metabolite effects on cancer cells. Chen *et al.* observed an improvement in hepatocyte synthesis and metabolism, which improved the effects of cancer drugs in this multi-chip system. The field of LOCs is moving into a multi-system, multicellular, and integrated sensing era, evidenced by the plethora of works in multi-sensing platforms of LOCs, which are discussed in Sec. V E.

III. LOC DESIGNS THAT MIMIC LIVER CHARACTERISTICS

As the largest gland in the human body, the liver weighs about 1.4 kg (2.5% body weight) in the average adult,[77,78] making it impractical to mimic the liver mass in a LOC device. Nevertheless, blood flow characteristics provide a practical approach for *in vitro* hepatic mimicry. Dimensionless parameters can be used to describe the fluid flow and mass transport characteristics, such as Reynold's number (Re, inertial/viscosity),[79] Péclet number (Pe, convective/diffusive transport),[80] and Damköhler number (Da, diffusion/reaction timescale).[81] LOCs provide the ability to control and manipulate these dimensionless numbers to mimic human physiological conditions. Unfortunately, only a handful of studies have specifically reported these parameters, although they are considered essential for ensuring the reproducibility of LOC designs. Other features of LOCs should also be reported, such as shear stress (induced by flow over tissue surface), effective culture time, characteristics of culture media (particularly for co-culture systems), and surface coating of the culture substrate. We have provided an overview of current studies on LOCs which have reported some of these essential parameters (Table II) and hope that this can serve as a guide for future research to consider the inclusion of such data.

In this section, we discuss the progress of LOC development to mimic different liver characteristics, including models of different liver lobules and their microstructures.[82] This leads into a discussion of mimicking liver heterogeneity and drug metabolism using LOCs, followed by a discussion of multicellular co-culturing in LOC designs.

A. Blood supply of the liver results in heterogeneity

The liver is supplied with both nutrient-rich and nutrient-depleted blood, and its functions are supported by interconnected networks of veins and arteries. The liver has an extremely high metabolic rate and is responsible for nutrient uptake, protein synthesis, detoxification, and bile production. The minute structures of liver lobules, a hexagonal shape with a central vein in the center, were introduced in 1833 by Kierman.[83] The nutritious blood from the hepatic portal vein mixes with oxygenated blood (from hepatic arteries) in the sinusoids, a conduit for blood flow from the portal tract toward the central vein. The sinusoids are lined by endothelial cells wherein the space of Disse resides between the endothelial cells and the hepatic plates (cords of hepatocytes). The hepatocytes secrete bile which flows to bile ducts and ultimately leaves the liver to travel toward the duodenum.[78] These three components, the bile duct, hepatic artery, and hepatic portal vein, collectively form the portal triad, which is located at the six corners of the hexagon. Lymphatic vessels could also be observed at this location, making it the portal tetrad or portal tracts. Two other models have subsequently been introduced: portal lobules and hepatic acinus lobules. Both are commonly used to define the structural and functional units of the liver.[84] Each of these hepatic models has inspired different types of LOC designs to replicate liver characteristics.

1. Portal lobules

The portal lobule can be identified as the basic unit of the liver by centering at the portal triad and connecting the three adjacent central veins, forming a triangular region [Fig. 3(i)]. The direction of blood flow at the portal lobule "diverges" from the portal triad to the central vein. Conversely, the flow of bile "converges" at the center. Such classification of liver units can be particularly useful when considering the exocrine (bile secretion) function of the cells.[85]

Ma *et al.* designed a chip [Fig. 3(iii)] that simulated the natural complexity of the liver microenvironment by integrating rapid 3D bioprinting with tissue engineering to construct physiologically relevant hexagonal units of liver cells and supporting cells (HUVECs and adipose-derived stem cells).[86] This hexagonal pattern directly imitated the classic lobule and portal lobule, which enabled improvements in the structure and function of hiPSCs-derived hepatic progenitor cells (HPCs). Both hiPSC-HPCs and supporting cells were found to recognize the designated lobular pattern and achieve cell–cell interactions in 3D tri-culture mode. The study suggested that this LOC could be used for early personalized drug screening and *in vitro* studies of liver pathophysiology.

2. Zoning of hepatic acinus

In 1954, another classification of liver units called hepatic acinus was proposed by Rappaport.[83] The hepatic acinus is identified by connecting central veins of two adjacent classic lobules with the adjacent portal triad, forming a diamond structure. Despite the apparent homogenous appearance on the histological level, the hepatic acini are regarded as heterogeneous at the subcellular level, as well as for biochemical and physiological functions. The hepatic acinus can be zoned into three tiers, Zones I, II, and III. The zonings are categorized by their proximity to the portal triad. Zone I is the closest to the blood supply, the first zone for receiving oxygen, nutrients, and toxins. Zone III is the furthest to the blood supply and the closest to the terminal hepatic central vein. Zone II lies between Zones I and III. The possibility of creating chemical gradients in LOCs to better recapitulate liver physiology inspires many designs.

Due to large variations in the distances of hepatocytes to the portal triad, a chemical and nutrient gradient can be observed in the hepatic acinus [Fig. 3(ii)(A)]. Variations such as enzyme activity and the size and number of cytoplasmic organelles are observed between Zone I and III. Cells in Zone II have intermediate functional responses and morphological characteristics compared to those in Zones I and III. Cells in Zone I are more resistant to the effects of nutritional deficiencies or circulatory compromises.[111] Upon circulation impairment in the hepatic lobules, cells in Zone I are the last to die and the first to regenerate. However, after bile duct occlusion (bile stasis), these cells are the first to show morphological changes.[112] Zone I is primarily responsible for ammonia detoxification and glucose metabolism processes.[113] Under reduced perfusion, cells in Zone III are the first to exhibit centrilobular necrosis and accumulate fat.[111]

Zonal differences could be seen in liver sinusoidal endothelial cells (LSECs). With the aid of transmission electron microscopy (TEM), the features of fenestrae were determined (Table III).[114–117] Wisse *et al.* reported the diameter of fenestrae to be around 107 ± 1.5 nm on the endothelial surface.[117,118] However, Zapotoczny *et al.* showed that different treatment of the tissue

TABLE II. Summary of the current literature on liver-on-a-chip (LOC): (1) type of device: solid organ chip—does not contain a membrane structure to mimic endothelial interactions, or scaffold-free, or barrier tissue—contains a membrane structure; (2) chip material; (3) substrate surface coating, (4) co-culturing (YES/NO); (5) cell lines used in the study; (6) length of the study; (7) operation flow rate and/or shear stress—also contains the values of the dimensionless parameters where mentioned; (8) application.

Reference	Type of LOC	Chip material	Substrate surface coating	Co-culturing (YES/NO)	Cell lines	Length of the study	Operation flow rate or/and shear stress	Application
Bhise *et al.*[73]	Solid organ chip	Multilayers of PDMS and PMMA glass——bottom	3-(trimethoxysilyl) propyl methacrylate	NO	HepG2 and C3A spheroids	Up to 30 days	200 μl/h	15 mM acute acetaminophen (APAP) exposure
Bonanini *et al.*[93]	Solid organ chip ——OrganoPlate® Graft	Top plate: virgin polystyrene. Bottom plate: optical quality 150 μm glass (1H coverslip thickness). Microfluidics: glass, proprietary polymers	Collagen I Matrigel GFR	YES	Cryopreserved Upcyte® human hepatocytes human primary RFP-labeled HUVECs (Alphabioregen, #RFP4)	7 days	On a rocker at + 14° and −14° inclination every 8 min	Vascularisation and experimentation of tissues *in vitro*
Boos *et al.*[94]	Scaffold free—hanging drop	PDMS	0.1% gelatin solution Biolipidure	YES	Primary human liver microtissues mouse embryonic-stem-cell line ES-D3	Up to 10 days	Spheroids generation on a rocker at ± 2° standing stop on a rocker at ±4°	Embryotoxic prodrug cyclophosphamide study
Bulutoglu *et al.*[95]	Solid organ chip	PDMS glass slide	50 μg/ml fibronectin	NO	Primary rat hepatocytes	Not mentioned	Not mentioned	Hypothesis testing about NAFLD progression
Chen *et al.*[92]	Solid organ chip	PDMS with glass slide	Not mentioned	YES	Hepa1–6 tumor spheroids JS-1 stellate cells	3 days	1 μl/min	Cancer cell stellate interactions under drug stimulation in a microchannel plate
Chen *et al.*[75]	Solid organ chip	PDMS	Collagen	YES	Human prostatic cancer cell (PC3) Mouse NIH/3T3 fibroblasts Human lung cancer cells (A549) Human breast cancer cells (MCF-7) Human liver cancer cells (HepG2) Primary rat hepatocytes	Not mentioned	30 μl/h flow rate 4.7×10^{-4} dyne/cm^2 shear stress	Testing for statin using prodrug simvastatin and active drug atorvastatin testing
Chhabra *et al.*[57]	Solid organ chip	Not mentioned	ECM	YES	Human primary hepatocytes	Not mentioned	On a rocker at ±25° at a frequency of 1 Hz 6.21 dyn/cm^2 shear stress	Not mentioned
Choi *et al.*[7]	Solid organ chip	PDMS	Pluronic F127	No	Primary rat hepatocytes	Up to 4 weeks	Static	Hepatic functions improvement
Corrado *et al.*[96]	Solid organ chip	Glass and polydimethylsiloxane	Not mentioned	NO	HepG2 μTPs HepG2 spheroids	14 days	Not mentioned	μTPs may be used to study the cytotoxic effects of xenobiotics
Delalat *et al.*[97]	Solid organ chip	Silicon and silicon dioxide	Potassium hydroxide	NO	Rat primary hepatocytes	4 weeks	90 μl/h	Microtrenches allow for maintenance of hepatocytes
Frey *et al.*[98]	Scaffold-free—hanging drop	PDMS	trichloro (1H,1H,2H,2H-per-fluorooctyl)silane	YES	Human colorectal carcinoma cells (HCT-116) Primary cell isolates from rat liver	Not mentioned	Maximal shear stress of 1.2 mPa Flow rate 10 μl/min Drop height 0.5 mm	Not mentioned

Gori *et al.*[99]	Solid organ chip	PDMS	Not mentioned	NO	HepG2	8 days	18 μl/day Negligible shear stress	Development of on-chip non-alcoholic fatty liver disease (NAFLD) models
Jang *et al.*[100]	Solid organ chip	OrganoPlate from MIMETAS and Leiden University	Matrigel	NO	HepG2	3 weeks	0.3 dyn/cm^2 shear stress	Cultivation of HepG2 cells
Jang *et al.*[101]	Solid organ chip	Not mentioned	ECM	NO	Primary rat, human, or dog hepatocytes Sinusoidal rat, human, or dog liver endothelial cells with or without Kupffer and/or stellate cells	14 days	10 μl/h	Not mentioned
Kang *et al.*[72]	Solid organ chip	PDMS	Collagen I 30% (v/v) Matrigel for RAMECs	YES	Rat primary hepatocytes and Endothelial cells (primary rat adrenal medullary and bovine aortic)	Up to 30 days	30–40 μl/h	Urea synthesis using diacetylmonoxime Viral replication for hepatotropic hepatitis B virus (HBV) and analysis
Khetani *et al.*[102]	Scaffold free—micropatterned	Tissue culture-treated polystyrene omnitrays (Nunc)	Collagen I	YES	3T3-J2 fibroblasts : Primary rat hepatocytes = 4:1	Up to 6 weeks	Static	Hepatic functions improvement
Kim *et al.*[103]	Scaffold-free—culture plate	PMMA	Pluronic127	YES	HepG2 HS68 fibroblasts Primary HUVEC	Up to 7 days	Mimetas Rocker kept at 7° angle and six rotation cycles per hour	Pro-inflammatory protein, IL-1β, used to induce inflammation
Lee *et al.*[104]	Solid organ chip	PMMA	Gelatin and liver dECM	YES	Human HepaRG cells Human umbilical vein endothelial cells (HUVEC)	Not mentioned	25 μl/min final flow rate	APAP used to check hepatotoxicity
Lee *et al.*[52]	Solid organ chip	Acrylic—- top PDMS—- middle Glass—bottom	Collagen I (10 μg/well) for mutiwell No coating for the LOC	NO	Rat and human primary hepatocytes	Up to 7 days	10–20 nl/min Re < 0.01 Pe = 56 in flow channel Pe = 0.8 in the barrier channel	Hepatotoxicity of the anti-inflammatory drug diclofenac
Lee *et al.*[70]	Solid organ chip	PDMS—- top PEGDA-microsomes—- middle Glass—bottom	Not mentioned	NO	Rat primary hepatocytes	Not mentioned	Tilt angle not mentioned 5 μl/min flow rate of substrate solution Pe > 1000	P450 reaction with microsome in solution phase tested with different substrate concentrations ranging from 2 to 80 μM
Lee *et al.*[71]	Solid organ chip	PDMS	3% (w/v) BSA Collagen I	YES	Rat primary hepatocytes and HSCs	Up to 13 days	5.53 mm/h flow speed	Live/Dead assay Albumin and urea secretion analyzed by measuring concentration in medium
Li *et al.*[105]	Barrier tissue	Polyethylene terephthalate —- middle glass-bottom	Fibronectin (100 μg/ml) Collagen (100 μg/ml)	NO	Human primary hepatocytes Human dermal microvascular endothelial cells Human stellate cells	Not mentioned	80 μl/h in heptic channel 100 μl/h in vascular channel	Induction of inflammation in liver diseases
Mazari-Arrighi *et al.*[106]	Scaffold-free-cell fibres	Glass bovine collagen I 10% Matrigel 1.0% Na-alginate 100 mM $CaCl_2$ 3% w/w sucrose solution	Not mentioned	NO	Primary rat hepatocytes	Up to 30 days	20 μl/min in the core 80 μl/min in the shell 3.6 ml/min in the sheath	Hepatotoxicity of the drugs acetaminophen and diclofenac

TABLE II. (*Continued.*)

Reference	Type of LOC	Chip material	Substrate surface coating	Co-culturing (YES/NO)	Cell lines	Length of the study	Operation flow rate or/and shear stress	Application
Moya *et al.*[107]	Barrier tissue	Glass-bottom	Collagen	NO	Rat and human hepatocytes	Not mentioned	Not mentioned	OOC devices including printed sensors allowing for real-time physiological measurements
Nakao *et al.*[69]	Solid organ chip	PDMS—- top Glass-bottom	Collagen Matrigel (150 μg/ml)	NO	Rat primary hepatocytes	Up to 4 days	1.36 mm/s at center of medium flow channel No flow in cell culture area 1.3 Pa (shear stress) in medium flow channel No shear stress in cell culture area	CDF excreted into bile canaliculi by MRP2 protein
Rennert *et al.*[91]	Solid organ chip	Multi-Organ-Tissue-Flow (MOTiF) biochip Cyclic olefin copolymers (COC)—TOPAS	COC-TOPAS® Plasma treatment	YES	HepaRG cells HUVECs Peripheral Blood Mononuclear Cells (PBMCs)	Up to 4 weeks	50 mPa·(0.5 dyn/cm^2) shear stress 50 μl/min perfusion rate	Not mentioned
Roth *et al.*[108]	Scaffold free—micropatterned	Polystyrene micropillar and microwell chip by MBD Korea	0.01% (w/v) PMA-OD attached PuraMatrix spots onto a micropillar chip	No	Human hepatoma (Hep3B)	Up to 3 days	Static	Adenoviral transduction and drug toxicity
Weng *et al.*[74]	Scaffold-free—micropatterned	PDMS	Collagen	NO	Primary liver cells (PLCs) and Primary HSCs	Up to 14 days	30 μl/min	APAP-induced hepatotoxicity
Yu *et al.*[109]	Barrier tissue	PDMS—- top Glass coverslip and parylene membrane—- middle Silicon—bottom						

APAP, acetaminophen; BSA, bovine serum albumin; CDF, 5-(and-6)-carboxy-2′,7′-dichloro-fluorescein; COC, cyclic olefin copolymers; dECM, Decellularized extracellular matrix; ECM, extracellular matrix; GFR, growth factor reduced; HBV, hepatitis B virus; HSCs, hepatic stellate cells; LOC, liver-on-a-chip; NAFLD, non-alcoholic fatty liver disease; PDMS, poly (dimethylsiloxane); PEGDA, poly(ethylene glycol) diacrylate; PMA-OD, poly(maleic anhydride-alt-1-octadecene); PMMA, poly(methyl methacrylate); RAMECs, primary rat adrenal medullary endothelial cells; μTPs, microtissue precursors.

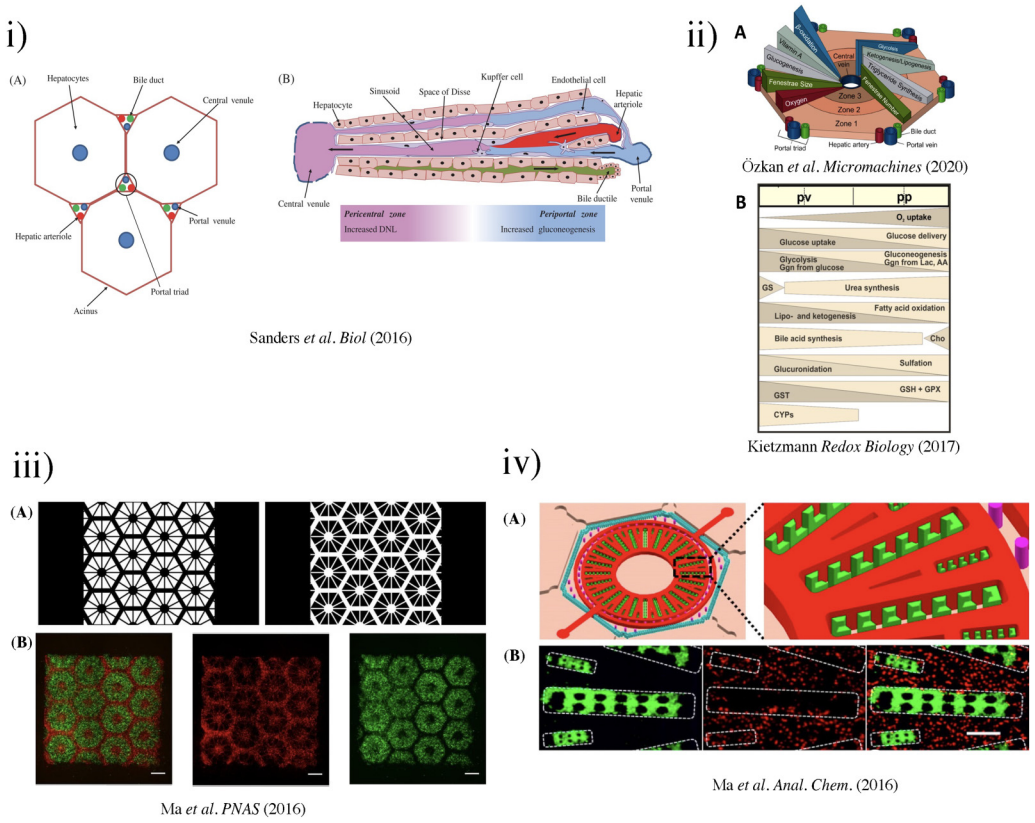

FIG. 3. (i) The liver acinus and zonation of metabolic processes. (a) The gross cytoarchitecture of the hepatic parenchyma. (b) A cross section of liver tissue along the porto-central axis demonstrates the proposed zonation of metabolic processes, with the pericentral zone as the primary site of *de novo* lipogenesis (DNL) and the periportal zone as the primary site for gluconeogenesis. As indicated by the arrows, blood flows from the portal area via the sinusoid into the hepatic venule. Bile flows in the opposite direction from hepatocytes to the bile duct through the bile canaliculi.[87] Reproduced with permission from Sanders *et al.* Biol. Rev. **91**(2), 452–468 (2016). Copyright 2015 John Wiley & Sons Ltd on behalf of Cambridge Philosophical Society. (ii) (a) Biochemical pathways, gradients, and endothelial properties alternation across the zones of the liver lobule. Reproduced with permission from Özkan *et al.* Micromachines, **11**(5), 487 (2020). Copyright 2020 MDPI.[251] (b) Distribution of major metabolic pathways. (pp, periportal; pv, perivenous; AA, amino acids; Cho, cholesterol synthesis; CYP, cytochrome P450 enzymes; Ggn, glycogen; Lac, lactate; GPX, glutathione peroxidase; GS, glutamin synthesis; GST, glutathione transferase.)[88] Reproduced with permission from Kietzmann *et al.*, *Redox Biology*, Vol. 11. Copyright 2017 Elsevier B.V. (iii) (a) Grayscale digital masks corresponding to polymerizing lobule structure (left) and vascular structure (right) are designed for two-step bioprinting. The white patterns represent the light reflecting patterns for photo-polymerization. (b) Images (5×) taken under fluorescent showing patterns of fluorescently labeled hiPSC-HPCs (green) in 5% (wt./vol) GelMA and supporting cells (red) in 2.5% (wt./vol) GelMA with 1% GMHA on day 0 (Scale bars, 500 μm).[86] (iv) Biomimetic microfluidic device with liver microarchitecture. (a) Schematic of the biomimetic microfluidic device with a hexagonal cell culture chamber, (b) morphological images of a single hepatic sinusoid-like structure with HepG2 cells and human aortic endothelial cell line.[89] Reprinted with permission from Ma *et al.,* Anal. Chem. **88**(3), 1719–1727 (2016). Copyright 2016 American Chemical Society. (v) (a) The microfluidic device prototype with four medium inlets/outlets (ABCD) and six cell culture wells. The width of the cell culture well ranges from 1 to 6 mm. (b) The top channel of the microfluidic device prototype was filled with the red dyes. (c) The zoom-in picture of the acinus-like culture well with the multi-row square-pillar PDMS microstructure with the trapped air. (d) The design sketch of the three rows microstructure.[90] Reproduced with permission from Shin *et al.*, Biomed. Microdevices **15**(5), 767–780 (2013). Copyright 2013 Springer Nature. (vi) Measurement of oxygen saturation in the cell culture medium by fluorescence emitting sensor spots. Top: Integration of oxygen sensor spots in the microfluidic biochip. Sensor spots were integrated at the inlets (1, 3) and the outlets (2, 4) of the upper and lower channel systems, respectively. Establishment of a three-dimensional liver model in a microfluidic biochip. Middle: Cross section of the biochip-embedded liver model.[91] Reproduced with permission from Rennert *et al.*, Biomaterials **71**, 119–131 (2015). Copyright 2015 Elsevier Ltd. All rights reserved. (vii) (a) The photograph of the fabricated microchip. (b) Scanning electron microscope (SEM) images of the concave microwell. (c) The scheme of cell aggregation and spheroid formation in the microwell. C1–C6, cell clture chamber 1–cell culture chamber 6.[92] Reproduced with permission from Chen *et al.*, Analyst **144**(14), 4233–4240 (2019). Copyright 2019 the Royal Society of Chemistry.

sample might affect the measured sizes. Most studies have shown that the average diameters of fenestrae in Zone I are higher than in Zone III, and the number of fenestrae increases from Zone I to Zone III. The exact measurements are unknown due to technical difficulties, such as limited access to tissue samples and changes in the diameter and number of fenestrations after treatment with various agents (hormones, drugs, and toxins). Despite this, the zonal variations of fenestrae are proven to play critical roles in gene therapy.[118] These physical measurements could be a guide for constructing *in vitro* models of the fenestrae of liver sinusoids.

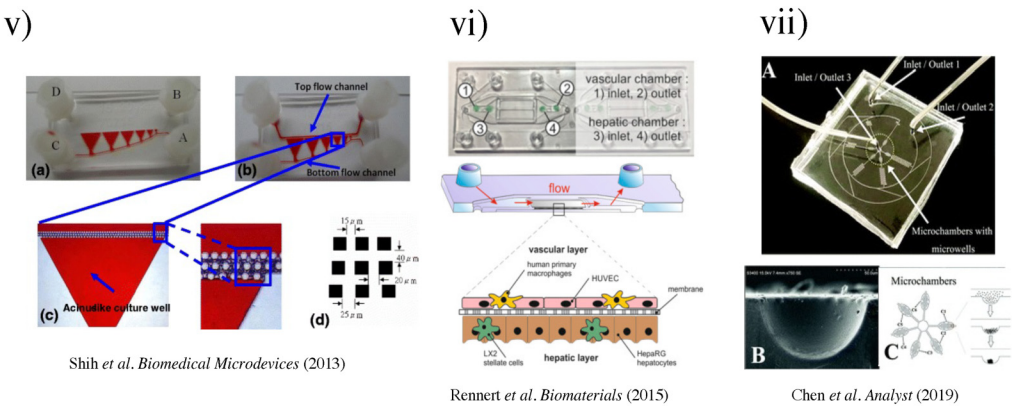

FIG. 3. (*Continued.*)

In 2013, Shih *et al.* designed a gradient microphysiological system that mimicked liver acinus by adopting three mechanisms.[90] First, PDMS was used to host the cells as a hydrophobic and gas-permeable material. Second, cell–cell interaction was encouraged by reducing the drag force during cell seeding, where the chip contained a multi-row square pillar [Fig. 3(v)] to balance the shear stress and mass transfer perfusion of the culture medium. Third, a reduced flow speed was enabled by connecting the top and bottom flow channels to achieve a concentration gradient. A non-linear concentration gradient was achieved by semi-circle flow design where the crossflow and the expansion phenomenon were balanced. Shih *et al.* inspired the creation of the biomimicry approach for LOCs.

3. Metabolic zonation

The concept of "metabolic zonation" was formally acknowledged by the work of Jungermann and Sasse in 1978.[123] This was derived from previous studies of carbohydrate metabolism, suggesting opposing metabolic pathways such as gluconeogenesis (or glucogenesis) and glycolysis are simultaneously occurring in hepatocytes in the periportal and perivenous regions, respectively.[119–126] Key chemical/metabolic gradients are present across the three zones [Fig. 3(ii)]. For example, oxygen and nutrient concentrations decrease from Zone I to Zone III, directly impacting the liver's functional adaptation to meet the various nutritional and energetic requirements for supporting metabolic pathways. Ma *et al.* described a biomimetic design to recapitulate the liver's metabolic zonation, by mimicking the hepatic cord network and hepatic sinusoid network [Fig. 3(iv)].[89] Using hepatic enzyme assay, it was found that the chip maintained high basal CYP-1A1/2 and UGT activities, indicative of great drug metabolism capacity. The chip also successfully predicted potential adverse reactions from clinical pharmaceuticals causing drug-induced liver injury, suggesting an application in the *in vitro* assessment of drug-induced hepatoxicity.

B. Multicellular co-culturing

A rich population of specialized cells supports the functions of the liver, classified into two categories: parenchymal cells (hepatocytes) and non-parenchymal cells (all other cells).[26] To build more physiologically relevant LOCs, co-culturing of parenchymal and non-parenchymal cells has been established for liver function evaluation and mechanistic studies. Monocellular culturing of hepatocytes can lead to shortened preservation of cellular morphology and functionality, finite perfusion duration,

TABLE III. Compiled data from various sources on the measurement of fenestrae.

Diameter (nm)		Density (per area, μm^2)			
Zone I	Zone III	Zone I	Zone III	Sample	Reference
150–175	NA	9	13	Unknown	Gebhardt 1992 Pharmacol. Ther.[119]
111 ± 0.25	105 ± 0.22	9	13	Rat liver	Wisse *et al.* 1985 Hepatology[120]
NA	NA	19	23	Human liver; non-alcoholic	Horn *et al.* 1987 Hepatology[121]
NA	NA	8.5	12	Human liver; alcoholic	Horn *et al.* 1987 Hepatology[121]
107 ± 1.5	NA	NA	NA	Human liver	Wisse *et al.* 2008 Gene Ther.[118]
180 ± 41	NA	NA	NA	Murine liver	Zapotoczny *et al.* 2017 Sci. Rep.[122]

diminished ECM-derived biochemical signals, and loss of cell polarity. The inclusion of non-parenchymal cells creates biomimetic tissue structures that allow hepatocytes to be subjected to native biophysiological–biophysical cues, enabling better modeling of liver homeostasis and functions.[18] Multi-cellular seeded chips have been shown to provide a more realistic physiological or disease model of the liver, and higher accuracy in predicting toxicity.[65–75]

To overcome the rapid loss of hepatocyte cell polarization and unwanted differentiation in static culture, Rennert *et al.* established a Multi-Organ-Tissue-Flow (MOTiF) perfusion microfluidic system together with co-culturing [Fig. 3(vi)].[91] By incorporating HUVECs (to mimic liver sinusoidal endothelial cells), monocyte-derived macrophages (to mimic Kupffer cells), and immortalized human hepatic stellate cells (LX-2) with HepaRG (immortalized hepatic cell line), the perfused liver organoid showed close resemblance to the morphological and functional characteristics of the human liver. This system could provide a continuous supply of oxygen and nutrients, and real-time monitoring of cellular oxygen consumption through the use of luminescence-based sensor spots. The oxygen consumption of HepaRG cells was studied at different media perfusion rates (1–3 μl/min) and found to increase at higher perfusion rates. These dynamic responses suggested that the MOTiF biochip could mimic *in vivo* conditions, making it a valuable tool for studying liver physiology, metabolism, and underlying molecular processes.

It has been reported that HSCs are a major component of the hepatic tumor microenvironment, and play critical roles in cancer progression as well as drug resistance. To elucidate the effects of HSCs (JS-1) on hepatic tumor spheroids (Hepa1–6), Chen *et al.* developed a microchannel plate-based co-culture model and used it to study drug resistance and cellular interactions.[92] The *in vivo* tumor microenvironment was set up using 3D concave microwells, recapitulating epithelial-mesenchymal transition and chemoresistance. The design incorporated a concentration generator to study the spatial and temporal stability of the LOC [Fig. 3(vii)]. This system facilitated the formation of hepatic tumor spheroids with simultaneous ability to monitor cell morphology, behavior, and other physiological changes under continuous flow.

IV. FABRICATION TECHNIQUES FOR LOC

To benefit readers from a wide range of disciplines interested in self-fabricating LOCs, we have provided a summary of the general procedures in fabricating LOC devices, drawing on recently published protocols and other comprehensive reviews. We hereby

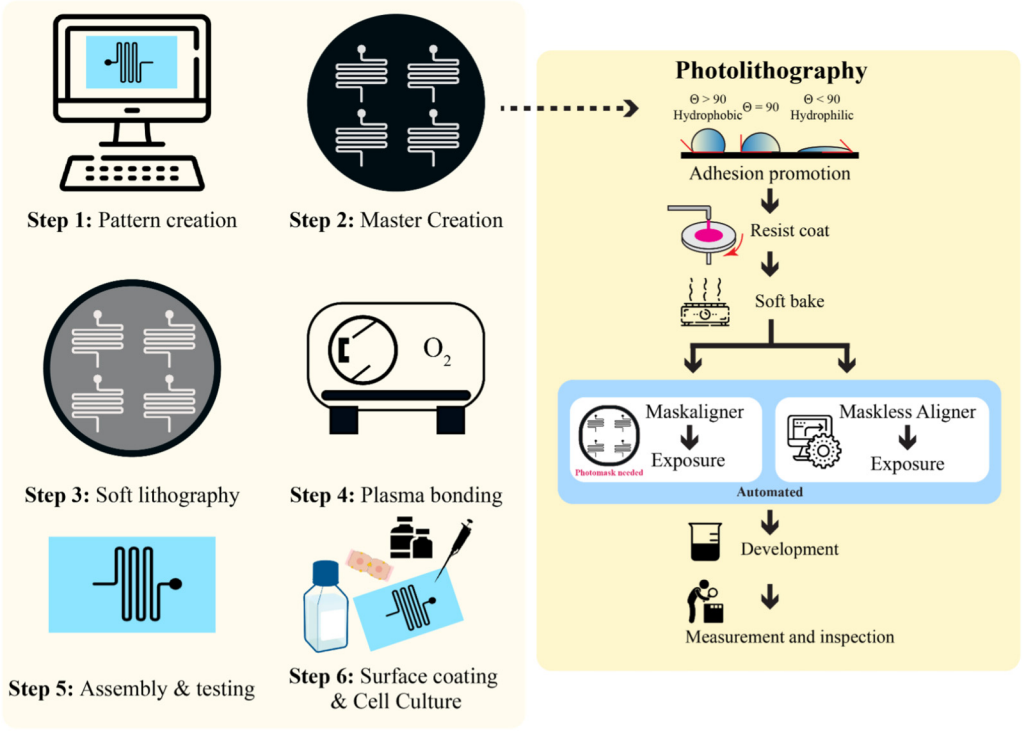

FIG. 4. A general procedure for creating a microfluidic LOC device in six steps. Step 1 is pattern creation, usually performed using computer-aided design software, such as AutoCAD. Step 2 is creating a master template on a silicon wafer where there is a choice of mask photolithography or maskless photolithography. Step 3 is the fabrication of the device by soft lithography. Step 4 is the plasma bonding of the chip materials. Step 5 involves the tube insertion and testing of the device before cell culturing. Step 6 shows the coating of the chip channels and the seeding of cells.

provide a graphical overview in Fig. 4, including recent advances in lithographic techniques and LOC-specific procedures. For detailed protocols, readers are encouraged to seek further details in other reviews.[39–127]

A. The general procedure to produce LOC devices

LOC devices have been combined with biosensors to achieve real-time monitoring of hepatocyte morphology and functions.[128,129] For continuous monitoring, LOCs need to sustain the phenotype of hepatocytes, particularly primary cells, and liver-specific functions in long-term culture.[130] In most LOC devices, multi-cellular or co-culturing has seen better and more accurate responses to drug testing and toxicological evaluations compared to 2D *in vitro* models.[131] The versatility of designing microfluidics patterns meets the needs of different research focuses, such as pathological studies and drug development.[55–59] In this section, we give an overview of the common procedures for fabricating LOC devices. Then, we specifically discuss emerging trends in cell fabrication techniques that have been incorporated for LOC technologies.

The general procedure for producing LOCs devices is outlined below:

(1) Create the desired pattern using computer-aided design (CAD) software with consideration of positive or negative imprint.
(2) Use photolithography techniques to create a master (or mold). The alternative method, maskless lithography, is discussed in Sec. IV B.
(3) Adopt the soft lithography technique to create a polymer-based LOC.
(4) Device bonding by plasma treatment.
(5) Microfluidics device evaluation and testing.
(6) Surface treatment of the materials for cell culturing to provide a functional LOC.

TABLE IV. Comparison between the types of photomasks and their pros and cons.[136,137]

Type of photomask	Advantages	Disadvantages
Quartz photomask	High resolution (>= 1.0 μm) Very stable Low thermal expansion coefficient Easy to clean Non-restricted wavelength range (> 180 nm)	Could break Very expensive Time consuming
Glass (soda lime) photomask	Cost-effective solution Stable Easy to clean High resolution (>= 2 μm)	Fragile Limited wavelength range (> 350 nm) Time consuming
Plastic photomask	Cheapest option of all Very easy to handle Rapid prototyping method Flexible Thin	Weak stability Low resolution (> 6 μm) Limited wavelength range (> 350 nm)

B. Photomask lithography and maskless lithography

Photomask lithography is solely dependent on the use of photomasks. Hereby, we summarized the different types of photomasks and their characteristics in Table IV. The typical costs of a photomask can range from the most expensive quartz (~USD$500, 5 in.) down to the least expensive plastic film (~USD$100, 9 × 12 in.) per photomask. The cost increases with size and resolution, as well as other handling expenses such as shipping (also extends the time needed for such fabrication process). One photomask may accommodate multiple designs at once, thus bringing down the cost per design. Typically, several iterations are required to produce an optimal LOC device. With any modification to the design, a new photomask needs to be procured. Efforts have been made to shorten the processing time and lower the cost by adopting techniques mentioned in other studies and reviews.[132–135] Here, we discuss a recent advance in photolithography using a maskless aligner, which completely abandons the use of photomasks.

With advances in instrumental designs, maskless lithography has become an option to perform rapid prototyping of microfluidics.[138] Maskless lithography relies on the use of a maskless aligner (MLA), such as Heidelberg MLA150.[139] The MLA150 can pattern features down to 0.6 μm with topside and backside alignment features. The maximum exposure area of MLA150 is $150 \times 150\ \text{mm}^2$. Using MLA150, microfluidic devices can be fabricated without the need to produce or outsource photomasks. In a recent study by Kasi *et al.*,[139] maskless photolithography was used to produce an OOC device capable of culturing human-induced pluripotent stem cell (hiPSC)-derived vascular cells and neuron cells. They also achieved a cleanroom-free microfabrication process, one step closer to an accessible and practical method for making microfluidic devices. Rapid prototyping with maskless photolithography offers opportunities for researchers to adopt it as a regular practice to produce high-fidelity and high-resolution microfluidic devices with shortened time frames and without the expenses of photomasks. The use of MLA is ideal for rapid prototyping during design-testing iteration cycles.

C. Soft lithography and surface functionalization

Duffy and Whiteside *et al.* introduced soft lithography in 1998.[68] This procedure is defined as micromolding an elastomeric polymer to generate a pattern, by replica-molding from a microfabricated master typically produced by photolithography. Hence, soft lithography is an auxiliary microfabrication technique to produce microfluidics devices.[61–142] Soft lithography is endorsed by researchers as an inexpensive way of fabricating microfluidics.

Over the years, PDMS has become one of the most commonly used materials in soft lithography. PDMS can achieve fidelity of below 0.1 μm.[143] Since PDMS is optically transparent above 240 nm, it is a suitable material for optical detection between 240 AND 1100 nm. PDMS is considered an insulator that allows circuits to be embedded, and its elasticity is tunable with a typical value of ~750 kPa. Due to its excellent biocompatibility, PDMS is the preferred material for rapid prototyping of microfluidic devices. Nevertheless, PDMS can absorb hydrophobic biological molecules and be incompatible with certain organic solvents.[144] To overcome

these issues, alternative elastomers have been adopted, such as polyester elastomers, tetrafluoroethylene-propylene elastomers, and thermoplastic elastomers.[145]

The general steps to produce a microfluidic chip using soft lithography are described as follows: (i) PDMS casting and thermal annealing at 40–70 °C or at higher temperature for a shorter curing time; (ii) PDMS chip peeled off from the mold and cut into the desired shape; (iii) creation of inlets and outlets of the assembled device using biopsy puncher; (iv) sealing the device by plasma bonding where different layers of design and a glass slide are joined together.[127] PDMS can be sealed to another PMDS block or other surfaces reversibly or irreversibly, making multi-layered device design possible. An alternative method, such as corona discharge, can be performed to achieve the same result.[146]

Surface treatment of the device may be necessary to promote cell adhesion or other processes such as spheroid production, enhance biocompatibility, and reduce chemical diffusion into the polymer material. In 3D spheroid cultures, pluronic acid is usually used to prevent undesired spheroid dissociation due to potential cell attachment to the surface. Other coatings such as proteins and ECM can promote cell attachment to the surface. Readers are encouraged to seek further information from other recently published reviews.[39–148]

D. Long-term cell culturing techniques

Primary human hepatocytes are considered the gold standard for *in vitro* cell culture to study liver characteristics and function. However, they are prone to rapid death *in vitro* in 2D culturing platforms. A key characteristic of LOCs is to achieve long-term culture of hepatocytes (over two weeks of continuous culturing) to address common issues such as contamination, clogging, and bubble accumulation in the chips, which can cause deterioration of cell function. This section reviews some of the current techniques to enable long-term cell culture in LOCs.

1. Production of 3D spheroids

As conventional spheroid culture is performed in static conditions, the depletion of nutrients around the spheroid periphery is inevitable, causing cell death at the center of the spheroids. Liquid overlay techniques have been used to produce a non-adherent surface for cells to form 3D spheroids, such as the use of poly-2-hydroxyethyl methacrylate (Poly-HEMA),[149] pluronic acid,[150] or 1–2% agarose coating on the substrate surface.[151] To improve the throughput, spheroids have been cultured with various techniques and in conjunction with LOCs. Spheroid LOCs can be realized by two general approaches: (1) produce spheroids using cell culturing techniques and then transfer the cell aggregates into LOCs and (2) direct production of spheroids in the LOCs. Several methods have been explored to produce spheroids, such as the use of ultra-low attachment (ULA) surfaces, bioreactors, hanging drops, microarrays, and the most recent developments in microfluidic spheroid formation chips—a technique for on-chip formation of spheroids.[152]

Kim *et al.* designed and fabricated a polymethyl methacrylate (PMMA) based hemispherical well-shaped cell culture chamber that was functionalized with a pluronic coating (1% w/v in water) to encourage cell aggregation [Fig. 5(i)].[103] The hepatocyte cell line HepG2, primary human umbilical vein endothelial cells (HUVECs), and fibroblast cell line H368 were adopted in the ratio of 5:4:1. The spheroids, with dynamic fluid flow caused by a rocker at 7° tilt and a rate of six rotations per hour, were exposed to IL-1β (1, 5, 10, and 20 ng/ml) over 5 days to cause cellular stress and produce an inflammatory disease model. Although this model demonstrated the possibility of simulating the hepatic microenvironment and human liver physiology in disease, there was lack of control over the dynamic fluid flow. Precise control of fluid flow could be introduced by the use of syringe pumps, peristaltic pumps, pressure controllers, or other types of fluid control devices.

In an early study by Tostões *et al.*,[153] a perfusion-stirred tank bioreactor was used to promote the formation of primary human hepatocyte spheroids ($81 \pm 4\,\mu$m diameter, week 2) during the first 72 h of culture. With proper controls, the bioreactor [Fig. 5(ii)] achieved convective mass transfer and environmental control appropriate for the robust formation of hepatic-like microtissue units. In this study, the primary human hepatocyte spheroids could maintain hepatic liver-specific synthesis, drug-metabolizing enzyme gene expression and activity, and liver-like architecture inside the spheroids for 2–4 weeks.

2. Hanging drop for LOC

The hanging drop method is an elegant use of the Young–Laplace equation[155]

$$\Delta p = \frac{2\gamma}{r}, \tag{1}$$

where p denotes the pressure, γ denotes the interfacial energy (air–liquid), and r denotes the droplet's radius. This cell fabrication technique relies on accumulating cells at the liquid–air interface to develop spheroids. There is an emergence of commercial hanging drop plates (HDPs) on the market, allowing the streamlined production of spheroids.[156] Disadvantages of such methods include the inability to use large liquid droplets (>50 μl) and the inability to change media without adversely affecting the spheroids.

To tackle the inability of media exchange during spheroid formation, Frey *et al.* presented a highly versatile analytical platform for forming multi-cellular spheroids.[98] The microfluidic system is composed of hydrophobic rims and circular chambers. Capillary forces drive the liquid from the inlet to the outlet, and as the pressure increases, the droplet builds up in size. As the bottom surface is the liquid–air interface, gas exchange and fluid dynamic profiles differ from closed microfluidic channels. The maximal flow velocity was found at the liquid–air interface [Fig. 5(v)]. This configuration offers the advantage of washing away unwanted single cells and debris. Frey *et al.* also achieved parallel spheroid formation by designing connecting ports (capillary valving), enabling the liquid flow without crossover. By introducing a small volume of liquid, the capillary valve broke, and the liquid would infuse together to create connected streamlines. By incorporating gradient microfluidics, different cell culturing media could be prepared. This array configuration allowed the rapid production of individual hanging

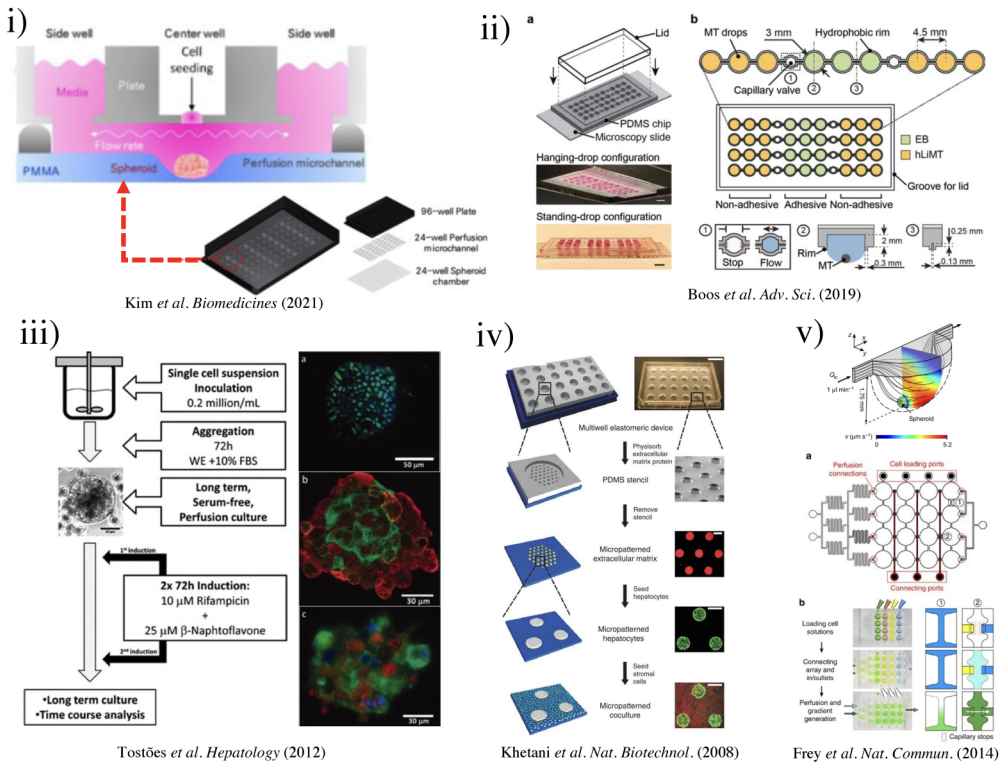

FIG. 5. (i) Schematic of three-well array for the gravity-based spheroid culture.[103] Reproduced with permission from Kim *et al.,* Biomedicines **9**(10), 1369 (2021). Copyright 2021 MDPI. (ii) Microfluidic multi-tissue hanging-drop platform. (a) The microfluidic network is patterned on the surface of a PDMS substrate. Photographs of the chip show its operation in hanging-drop and standing-drop configuration. Scale bar: 5 mm. (b) The chip layout consists of four individual lanes of nine interconnected drops.[94] Reproduced with permission from Boos *et al.,* Adv. Sci. (Weinh) **6**(13), 1900294 (2019). Copyright 2019 John Wiley& Sons. (iii) Experimental design of the induction of the CYP450 enzymes in primary cultures of hepatocyte spheroids in the bioreactor (left). Scale bar = 50 μm. Immunofluorescence microscopy of liver-specific antigens in human hepatocyte spheroids after two weeks of bioreactor culture (right).[153] Reproduced with permission from Tostões *et al.*, Hepatology **55**(4), 1227–1236 (2012). Copyright 2011 John Wiley & Sons; (iv) schematic of the process flow aside photomicrographs taken at each step. A reusable PDMS stencil is seen consisting of membranes with through-holes at the bottom of each well in a 24-well mold. Primary hepatocytes selectively adhere to matrix-coated domains, allowing supportive stromal cells to be seeded into the remaining bare areas (hepatocytes labeled green and fibroblasts orange; scale bar is 500 μm).[102] Reproduced with permission from Khetani *et al.,* Nat. Biotechnol. **26**(1), 120–126 (2008). Copyright 2007 Springer Nature. (v) Numerically simulated streamlines and flow velocities of a perfused drop containing a 400-μm-diameter spheroid (the applied flow rate is 1 μl min^{-1}; hanging drop has maximal size and a height of 1.75 mm). The same flow rate is applied at the outlet. Gray areas indicate contact walls with the no-slip condition (v = 0 μm s^{-1}). (a) Layout of the four-by-four drop array, showing the added features for array reconfiguration (marked in red). (c) Three handling steps are required during an experiment (close-up views show key areas).[98] Reproduced with permission from Frey *et al.,* Nat. Commun. **5**(1), 4250 (2014). Copyright 2014 Springer Nature. (vi) Schematic representation of the micropillar and microwell chip platform for use in Hep3B cell encapsulation in PuraMatrix and compound toxicity assessment.[108] Reproduced with permission from Roth *et al.,* Mater. Sci. Eng. C **90**, 634–644 (2018). Copyright 2018 Elsevier. (vii) Encapsulating primary rat hepatocytes within core–shell hydrogel microfibers by applying cell fiber technology. (a) Schematic drawing of the fabrication of core–shell hydrogel microfibers encapsulating freshly isolated rat hepatocytes through a double-coaxial microfluidic device. (b)–(g) Representative dark-field images (n = 12 cell fibers for each group) of primary rat hepatocytes encapsulated in cell fibers before culture and after 48 h of culture in three experimental groups possessing different initial cell seeding densities: 2.5, 5, and 9 × 10^7 cells ml^{-1}. Scale bars; 100 μm.[106] Reproduced with permission from Mazari-Arrighi *et al.,* Sci. Rep. **12**(1), 1–12 (2022). Copyright 2022 Springer Nature. (viii) Design principles of tissue incubator. (a)–(d) Schematic diagram of design principles. (e) Photo of entire device. (f) Schematic diagram of radial flow. (g) LOC shows good cell viability with Calcein AM staining (green).[74] Reproduced with permission from Weng *et al.,* Adv. Mater. **29**(36), 1701545 (2017). Copyright 2017 John Wiley& Sons. (ix) The OrganoPlate Graft allows for the generation of robust microvascular beds. (a) Top and bottom views of the OrganoPlate Graft with 64 microfluidic units positioned underneath a 384 microtiter plate. Each microfluidic unit makes use of a 2 × 3 array of wells from the microtiter plate (the inset image). (b) Sequence of steps for generating a microvascular bed.[93] Reproduced with permission from Bonanini *et al.,* Angiogenesis **25**(4), 455–470 (2022). Copyright 2022 Springer Nature. (x) Developed micropatterned devices. (a) Schematic of the microgrooves-based platform with pink: liver compartment and gray: tumor compartment; (b) picture of the microgrooves-based device and stamp for micropatterning; (c) concept of the valve-based platform with pink: liver compartment and gray: tumor compartment. In the zoom is shown the valve operating principle; (d) a picture of the valve-based device.[154] Reproduced with permission from Ferrari *et al.*, Biomed. Mater. **16**(4), 045032 (2021). Copyright 2022 IOP Publishing, Ltd.

drops with metabolic cross-communication between spheroids. They successfully demonstrated the ability to culture primary rat liver microtissues (rLiMT) in parallel with human colon cancer cell line HCT-116.

In a recently developed device by Boos *et al.*,[94] the hanging drop method produced embryonic bodies (EBs) and primary human liver microtissues (hLiMTs) to integrate liver metabolism into the embryonic stem cell test (EST). The hanging-drop-network [Fig. 5(ii)] was

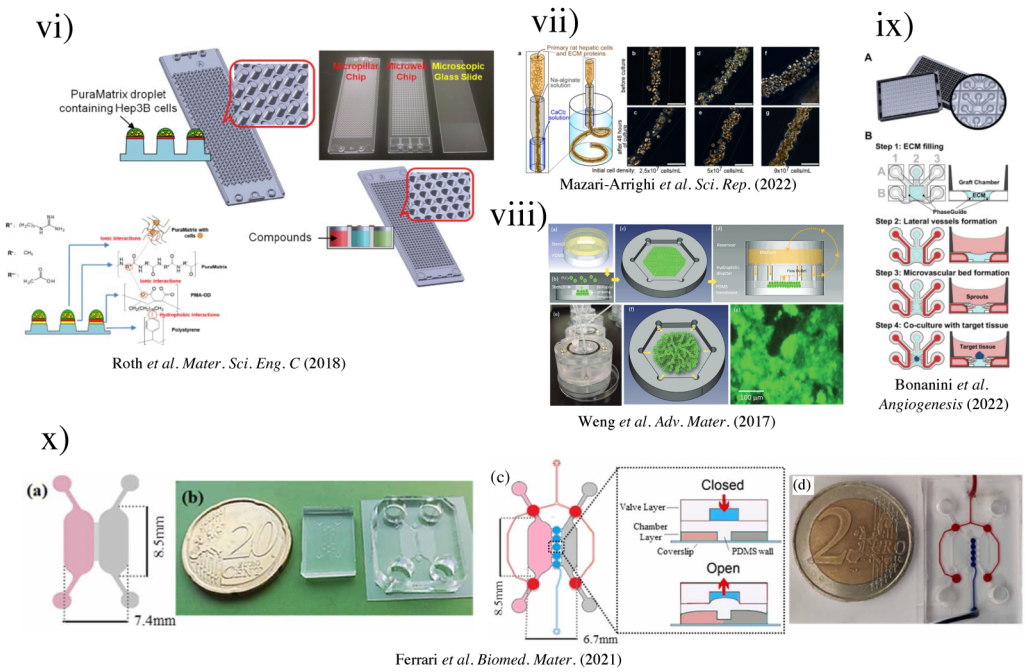

FIG. 5. (*Continued.*)

used to co-culture EBs with hLiMTs in immediate proximity to each other, named "metaEST." During EB formation, hLiMTs were disconnected from EB due to the presence of the hydrophobic rim and capillary valve under static culturing conditions. After 24 h, the wetting of the capillary valve established liquid exchange between the compartments, and fluid flow was induced by slightly titling the chip by ±2° every 15 s with an average turnover of 4.5 μl per tilting cycle for 5 days. On day 5, the chip was flipped upside-down to obtain a standing-drop configuration and tilted at ±4° every 15 s with an average medium turnover of 8.7 μl per tilting cycle. Due to different coatings of the substrate, hLiMTs remained spheroids, whereas the EBs adhered and spread on the adhesive surface. As proof of concept, the drug cyclophosphamide was used, which showed a fourfold lower ID50 concentration after biotransformation, demonstrating the metaEST as a promising tool for EST.

3. Microarrays

Another emerging technique to produce spheroids for LOCs is using microarrays. The aforementioned techniques for spheroid production by ultralow attachment 96-well plates and hanging drops have the disadvantages of low throughput, challenging operations, and being labor intensive.[157,158] To improve throughput, a microwell microarray has been proposed by Chao *et al.* by engineering the cell attachment surfaces with agarose gel.[159] A negative mold with microwell patterns of 250 μm diameter and 400 μm center-to-center spacing was created; approximately 160 microwells could fit into the bottom surface of a single microwell of the plate. A PDMS stamp with microarrayed pillars was created using the mold and subsequently set in the molten agarose over GelBond film (Lonza, 53761) for 15 min. By removing the PDMS mold, an array of microwells was created. The agarose gel was clamped between a 96-well bottomless plate and a glass plate while the cell loading was done. With the removal of the 96-well bottomless plate, the patterned agarose microwell microarray trapped HepG2 cells and encouraged the formation of HepG2 spheroids within 1–2 days. With this technique, Chao *et al.* further modified the assay to show that intact HepG2 spheroids cultured in microwells could be electrophoresed to reveal the extent of DNA damage following exposure to inflammatory chemicals, such as H_2O_2 and SIN-1.

The use of hydrogel scaffolding can accelerate and maintain cell growth in microarray systems. For instance, incorporating hydrogels on top of the micropillars in the microarray can improve their surface chemistry. Key advantages of coating the pillars with hydrogels are the improved high-throughput screening of potential drug candidates, diffusion of nutrients, and imaging of cells. Roth *et al.* explored the use of PuraMatrix as the hydrogel matrix,[108] which made the study of viral transduction possible [Fig. 5(vi)]. The surface chemistry of micropillars was optimized by a coating of poly(maleic anhydride-alt-1-octadecene) (PMA-OD, 0.01% w/v in ethanol) and subsequently printed PuraMatrix (0.25% in water) using the S + microarrayer at 60 nl/micropillar. Six model compounds, acetaminophen, lovastatin, rotenone, tamoxifen, menadione, and sodium citrate, were tested on 3D-cultured Hep3B cells for rapid toxicity assessment by obtaining IC_{50} values. With the improved surface chemistry, Roth *et al.* demonstrated the suitability

of the PuraMatrix hydrogel for 3D cell encapsulation, gene expression, and rapid toxicity assessment.

4. Microfluidic spheroid formation chips (μSFCs)

μSFCs refer to microfluidic chips that could promote the formation of spheroids in chips with the additional ability to maintain the culture of spheroids.[152] μSFCs have shown the ability to prolong the lifetime of hepatic cell lines (such as HepaRG, HepG2, and Fa2N-4) in culture and help preserve their phenotype, making them a promising *in vitro* model for evaluating hepatic metabolism and cytotoxicity.[160] To exploit the use of 3D spheroids in constructing LOC, Choi *et al.* produced a microfluidic device with a microstructured floor, containing pyramidal wells to promote primary rat hepatocytes in forming uniform assemblies of hepatic spheroids (~100 μm in diameter).[7] Two different sizes of pyramidal wells, a small size (4.25 μl with 100-μm headspace) and a large size (40 μl with 1600-μm headspace), and a 2D culturing platform were used, showing that hepatic spheroids in LOCs can enhance cell phenotype and function. More importantly, Choi *et al.* demonstrated that the geometry and mass transport of the cell culture system played an unequivocal role in the accumulation of autocrine signals and maintenance of primary hepatocytes. It was found that small-volume spheroid cultures were more robust. Compact spheroids formed over the course of 24–48 h showed significantly higher production of albumin, higher cytochrome P450 2A1 expression and the formation of bile canalicular networks within individual spheroids in small-volume microfluidic spheroid culture.

Another bottleneck in modeling human hepatic tissues *in vitro* is the ability to produce vasculatures in liver organogenesis and regeneration models. Bonanini *et al.* presented a viable approach to promote vasculatures for *in vitro* models, using an innovative design combining spheroids and a microfluidic vascular bed.[93] They created an OrganoPlate Graft, comprising patterned 64 microfluidic chips underneath a standard 384-well plate. Each chip had two perfusion channels and a gel channel [Fig. 5(ix)]. Two phaseguides at the bottom of the microfluidic channel served as a capillary pressure barrier and assisted in the filling of ECM gel. Collagen I was used to pattern the phasedguide at inlet A2 [Fig. 5(ix)(B)] for improved cell viability. A four-step procedure was adopted for *in vitro* tissue grafting, which achieved co-culture of HUVECs and cryopreserved Upcyte® human hepatocytes.

5. Matrix embedding

Hydrogels are the most common choice for cell scaffolding in constructing LOC because of their space-filling ability, controllable porosity and topography, and biocompatibility.[18–162] Novel methods such as electrospinning nanofibers have also been studied. 3D scaffolds made from a range of natural and synthetic materials have been used to help promote hepatocyte growth.[163,164] Using native ECM is another method for mimicking the native microenvironment of hepatocytes,[165] such as a decellularized liver scaffold by removing hepatocytes and non-parenchymal cells.[166] Studies have shown that decellularized ECM could provide a physiologically relevant environment with suitable biophysical and biochemical factors to encourage hepatocyte growth and function.[53–168]

To improve the longevity of primary hepatocytes during *in vitro* culture, Mazari-Arrighi *et al.* developed cell-laden core–shell hydrogel microfibers, named "cell fibers", that could maintain primary rat hepatocyte viability and liver-specific functions for up to 30 days in culture.[106] The cell fibers were generated using a double-coaxial laminar-flow microfluidics device, where the core contained both cells and ECM proteins (mixture of collagen I and Matrigel), while the shell was an alginate hydrogel. By varying the initial cell seeding concentration, cellular clusters would vary their morphology, whereby a lower cell density increased the likelihood of the cell cluster becoming spheroid shaped [Fig. 5(vii)]. Mazari-Arrighi *et al.* tested the performance of cell fibers in detecting drug hepatotoxicity using acetaminophen and diclofenac. Cell fibers allowed accurate estimation of the 50% inhibitory effect (IC50) for up to 30 days for these two drugs, representing a significant improvement compared to cells cultured in a 24-well plate. These cell fibers showed the possibility of offering scalability and handleability over long culture periods.

E. Other techniques

The fabrication of microfluidics devices is complicated and requires state-of-the-art facilities, such as a cleanroom, increases the relative cost of a LOC. Additive manufacturing including 3D printing allows complex structures to be built from various materials, for example, through layer-by-layer deposition of material ink.[169] Building up from this, 3D bioprinting enables the production of microfluidic devices incorporating cells in a one-step procedure.[170,171] This dramatically reduces the cost per chip and shortens the production time, making 3D bioprinting an attractive technique for rapid prototyping and proof-of-concept validation in constructing LOC.

Recent advances in 3D bioprinting allow the direct printing of viable cells with 3D tissue structures in a single continuous procedure with great accuracy.[172,173] 3D bioprinting techniques can be categorized further into stereolithography, inkjet, extrusion, and laser-assisted bioprinting. Different techniques can achieve varying degrees of cell viability, resolution, and printing speed. Two-step fabrication has been recently reported where the microfluidic chip is fabricated using a conventional microfabrication technique, followed by bioprinting cells into the prefabricated chip. Different bioinks have been developed to accommodate various OOCs including LOCs, as captured in recent reviews.[174,175]

Bhise *et al.* provided a novel model where human HepG2/C3A spheroids encapsulated in a hydrogel scaffold were bioprinted into a microfluidic device for hepatotoxicity testing.[73] The primary device comprised PDMS and PMMA, and spheroids were formed using microwell technique followed by suspending the cell clusters in gelatin methacryloyl (GelMA) hydrogel scaffold. Unlike other devices, this platform could be easily disassembled and reassembled during the experiment to allow access to the cells in culture. The tissue-like construct was assessed over 4 weeks, in conjunction with cellular response to acute acetaminophen exposure over 1 week for predicting drug toxicity. Results indicated a significant decrease in metabolic activity over 6 days in cultures with acetaminophen, similar to the hepatotoxicity response reported in animal models. This device was thought to provide a 3D culture environment to

study drug-induced toxicity *in vitro*, with high throughput and prediction capability comparable to *in vivo* conditions.

To reproduce the biliary system of the liver, Lee *et al.* used 3D bioprinting to create a fluidic structure with decellularized ECM bioink.[104] The device consisted of an upper channel for nutrient supply and a lower channel for bile salt secretion and waste removal. HepaRG cell line was used for the differentiation of hepatocytes and liver biliary-epithelial cells. HUVECs were incorporated to create liver sinusoids in the 3D bioprinted structure between the two channels. This LOC device was able to incorporate multiple cell types and create biomimetic vascular and biliary systems, and also showed an effective drug response when evaluated using acetaminophen.

Despite the potential of 3D bioprinting in creating biomimetic LOC designs, the success of this technique is limited by the printing resolution. More complex features, such as capillary networks, could be a challenging feature to be incorporated into the bioprinted structure. Increasing the printing resolution would also extend the printing time, and a balance needs to be considered to ensure cell viability during a prolonged printing process. Although high-fidelity 3D bioprinters exist, they could be expensive, which might defeat the purpose of rapid and economical prototyping.[176,177] Further advances in cell sources and printing technologies are required to realize the full potential of using bioprinting to create LOCs.

Recent developments in micropatterning also show promise as an alternative method for OOC fabrication. Khetani and Bhatia used an elastomeric PMDS stencil to culture human liver cells in multi-well format.[102] The stencil contained 300-μm-thick membranes with through-holes at the bottom of each well in a 24-well mold. The multi-well mold was sealed against a polystyrene plate. After applying collagen I to the exposed polystyrene plate, the stencil was removed, and the coated area could selectively support the growth of hepatocytes. After varying the diameter of collagen islands over several orders of magnitude, hepatocyte functions were found to be maximized using 500 μm islands with 1200 μm center–center spacing [Fig. 5(iv)]. The microscale architecture, where the hepatocytes were surrounded by fibroblasts, remained stable for several weeks in culture. Dose- and time-dependent chronic toxicity was demonstrated using troglitazone, characterized by TC_{50} (the concentration that produced a 50% reduction in mitochondrial activity after acute exposure) and morphological changes. This study successfully showed that micropatterning could be used for drug toxicity screening.

To further investigate the micropatterning capability, a multi-organs-on-a-chip was developed by Ferrari *et al.* based on the micropatterned technique proposed by Khetani and Bahtia.[154] Ferrari *et al.* created a micropatterned dual-compartment microfluidic device to co-culture human Caucasian hepatocyte cell line (HepG2) and murine embryonic fibroblasts (NIH–3T3) in the liver compartment and colon cancer cell line (HCT-166) in the tumor chamber, as shown in Fig. 5(x). Instead of a stencil, plasma ablation was used to create the coating patterns of collagen I (50 μg/ml, 300 μl) on glass slides using a PDMS stamp mask. Two different systems were developed, microgrooves (5 μm high, 3 μm wide, 1 mm long, and inter-channel gap 30 μm) and a valve system actuated by vacuum. Tegafur, a prodrug of 5-fluorouracil, was injected into the liver compartment to test the dual-compartment systems. This platform reproduced the metabolism of Tegafur in the liver and demonstrated the killing of colon cancer cells.

Using a different approach, Weng *et al.* developed a scaffold-free model by introducing primary hepatic stellate cells (HSCs) as a physiologically relevant organotypic culture [Fig. 5(viii)].[74] The cells synthesized physiological ECM within a specially designed tissue incubator device made using PDMS, which was later removed, enabling the construction of scaffold-free multiscale and hierarchical tissue structures. The formation of tissues showed close resemblance to natural hepatic morphogenesis. Nevertheless, these tissues lacked biliary structures which were essential for studying metabolic mechanisms.

V. APPLICATIONS OF LOCS AS MODELS OF LIVER FUNCTIONS

The translation of new drugs can often fail during clinical testing due to the absence of physiologically relevant and cost-effective models to predict drug toxicity and therapeutic effects. From data collected in the United States in 2014, the high failure rate of drug development at a striking 90% amounted to a cost of USD 2.59 billion,[178] due to inadequate screening in preclinical trials.[179] lOC could be a solution that mimics liver function to enable adequate preclinical testing of hepatic drugs. In this section, we surveyed recent advances in LOC designs for measuring drug metabolism and assessing nanotoxicity, and as pharmacokinetic models and multi-component sensing platforms for hepatic biomarkers.

A. Pathophysiological models

A number of LOCs were developed over the years as models to study liver pathophysiology. In one of the first models, Lee *et al.* designed a biomimicry microfluidic device that modeled hepatic sinusoids using primary rat and human hepatocytes.[52] It could use 100 times less cells per experiment compared to macroscopic hepatic organoids and achieve improved hepatocyte viability over 7 days. Endothelial-like barriers were designed to reduce shear stress by preventing direct fluid flow to the hepatocytes [Fig. 6(i)(A)]. This device encouraged cell–cell interactions and allowed mass transport of liver sinusoids to be closely studied. This study guided the design of future devices.

Nakao *et al.* focused on mimicking the microscopic structure of hepatic cords.[69] As freshly isolated human hepatocytes rapidly lose membrane polarity, they proposed a new technique for maintaining the cells based on Lee's design. The cell culturing channel was altered to become asymmetric and promoted the cells to self-organize into two lines [Fig. 6(i)(B)], creating a separate channel for bile secretion. This system was considered by the authors to have flow distribution similar to *in vivo* structures.

In an improved design by Jang *et al.*, separation of cell culture area and perfusion flow was achieved without physical barriers using OrganoPlate™, developed by MIMETAS and Leiden University [Fig. 6(ii)].[100] This microfluidic device had 40 culture chambers, where each chamber consisted of three lanes separated by phase-guides, allowing the generation of continuous passive perfusion without the need for an extra pump or tubing. Improved function of HepG2 cells was observed in the microfluidic chip compared to static 2D and 3D cultures. Capillary force directed the flow of HepG2 and Matrigel mixture in the inner channel along the

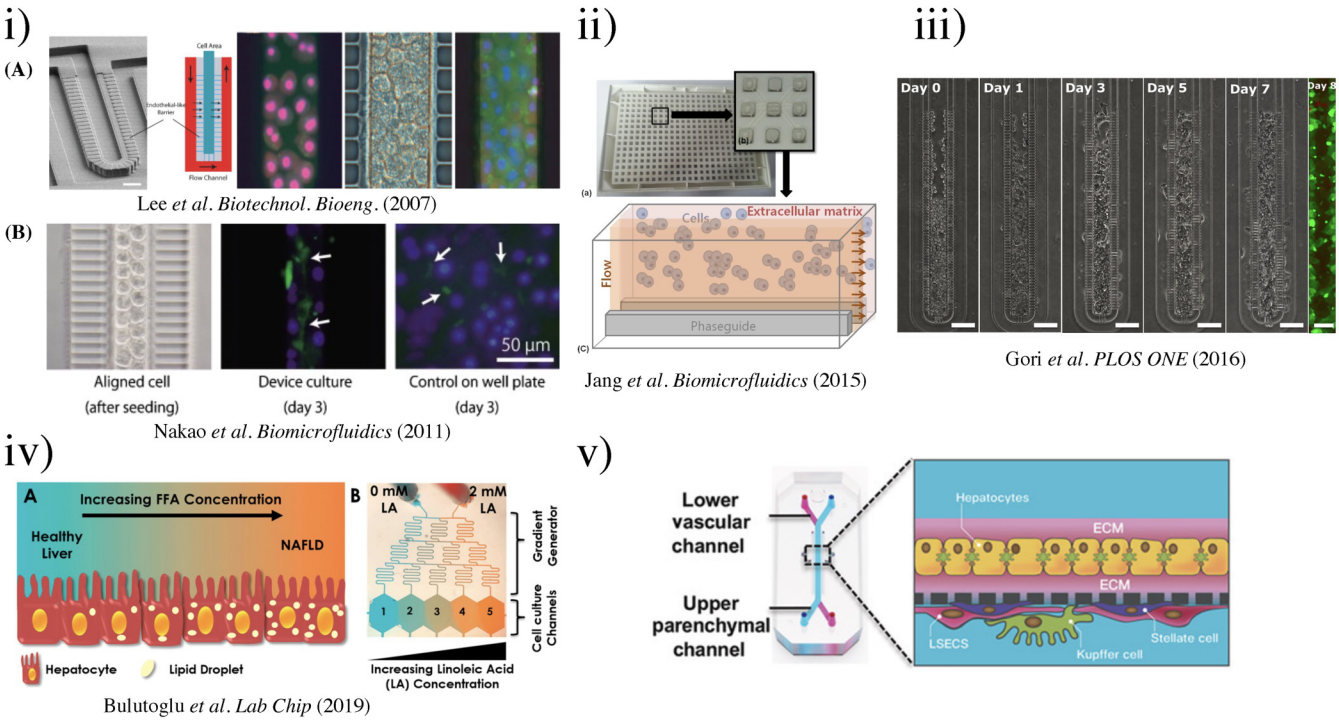

FIG. 6. (i) (a) SEM image depicting the microfluidic sinusoid unit. Scale bar represents 50 μm. Microfluidic culture of hepatocytes.[52] (Copyright 2007 Wiley Periodicals, Inc.); (b) results of cell alignment and culture. Left, aligned cells in two lines similar to a hepatic cord. Bile canaliculi were formed randomly in the well plate.[69] Reproduced with permission from Nakao *et al.,* Biomicrofluidics **5**(2), 022212 (2011). Copyright 2011 AIP Publishing LLC. (ii) Schematic presentation of the microfluidic device. (a) The microfluidic structure is embedded on the bottom of 364-well plates. (b) Each culture chamber has three lanes with an inlet and an outlet, respectively. (c) Culture model for HepG2 cells in an extracellular matrix separated from flow without any physical barrier using phaseguides. HepG2 cells have indirect contact to flow. Reproduced with permission from Jang *et al.,* Biomicrofluidics **9**(3), 034113 (2015). Copyright 2015 AIP Publishing LLC. (iii) Phase contrast micrographs of HepG2 cell growth inside the microfluidic sinusoid over a week in culture (Day 0, 1, 3, 5, and 7 are shown). Scalebar: 100 μm. On the right, fluorescence micrograph of live/dead assay performed at Day 8 (living cells in green, calcein dye; dead cells in red, EthD-1 dye; scalebar: 50 μm).[99] Reproduced with permission from Gori *et al.,* PLOS ONE **11**(7), e0159729 (2016). Copyright 2016 PLOS ONE. (iv) Schematics of the NAFLD development process and gradient microfluidics with the corresponding concentrations.[95] Reproduced with permission from Bulutoglu *et al.,* Lab Chip **19**(18), 3022–3031 (2019). Copyright 2019 the Royal Society of Chemistry. (v) Schematic of the liver-chip that recapitulates complex liver cytoarchitecture. Primary hepatocytes are grown in the upper parenchymal channel in ECM sandwich format, and non-parenchymal cells are grown on the opposite side of the same membrane in the lower vascular channel.[101] Reproduced with permission from Jang *et al.,* Sci. Transl. Med. **11**(517), eaax5516 (2019). Copyright 2019 The American Association for the Advancement of Science. (vi) Representation of the HepG2-μTPs loading procedure and fluid dynamic simulation.[96] (Copyright 2018 Wiley Periodicals, Inc.). (vii) 3D HepaTox Chip for the simultaneous administration of multiple drug concentrations. (a) Microfluidic design and assembly of the linear concentration gradient generator and multiplexed cell culture chip. (b) Magnified view of a single cell culture channel of the multiplexed cell culture chip. An array of 30 × 50 mm micropillars separated the channel into three compartments. (c) Characterization of the concentration gradient profile in the 3D HepaTox Chip coupled with a linear concentration gradient generator.[187] Reproduced with permission from Toh *et al.,* Lab Chip **9**(14), 2026–2035 (2009). Copyright 2009 the Royal Society of Chemistry. (viii) Functional maintenance of rat hepatocytes cell line (H-4-II-E) at a density of 1×10^5 cells ml^{-1} on silicon microtrenches (11 mm in length × 10 mm in width) with different depths of 10 and 20 μm, with and without heparin coating, under static conditions. Representative bioartificial liver (bottom)[97] (Copyright 2018 WILEY-VCH Verlag GmbH & Co. KGaA, Weinheim). (ix) Schematic of the perfusion-incubator-liver-chip (PIC). (a) 3D view with the PIC. (b) Bottom view of the chip's layout illustrating the microfluidic circuit, the cell culture chamber, the bubble trap, and the heater. (c) Cross section of the PIC illustrating the structure of the bubble trap. It consists of a 70 μm-thick PDMS membrane (gas permeable) bonded to a PDMS molded chamber with pillars that support the membrane. (d) Top and bottom views of the PIC.[110] Reproduced with permission from Yu *et al.,* Sci. Rep. **7**(1), 14528 (2017). Copyright 2017 Scientific Reports. (x) Vascular-liver PIC: (a) photo of the PIC, showing the glass–silicon chip, connectors, tubing, and media reservoirs and (b) cross-section schematic of the cell co-culture chamber. (c) Schematic of the bidirectional perfusion culture testing setup.[109] Reproduced with permission from Yu *et al.,* Biomicrofluidics **14**(3), 034108 (2020).Copyright 2020 AIP Publishing LLC. (xi) Model of molecular interactions in SHEAR. Cytokine stimulation combined with flow and IL-1β stimulates endothelial cells to produce PGE2, which plays an important role in the signaling cascade that leads to primary human hepatocyte cell-cycle entry in SHEAR devices.[57] Reproduced with permission from Chhabra *et al.,* Proc. Natl. Acad. Sci. U.S.A. **119**(28), e2115867119 (2022). Copyright 2022 PNAS.

phaseguide, which ultimately formed hepatic spheroids. The system was capable of preserving cellular viability and integrity for at least 15 days, demonstrated by the constant low lactate dehydrogenase activity in the cells and substantial increase of albumin production over this time. The LOC showed higher sensitivity for measuring the toxicity of acetaminophen than the monolayer control.

Other than mimicking physiological liver structure, LOCs can be used to create hepatic disease models. A prime example is non-alcoholic fatty liver disease (NAFLD), affecting millions of people worldwide.[180] This chronic disease can range from simple steatosis to non-alcoholic steatohepatitis, which may even progress to cirrhosis and eventually hepatocellular carcinoma (HCC).[181] The

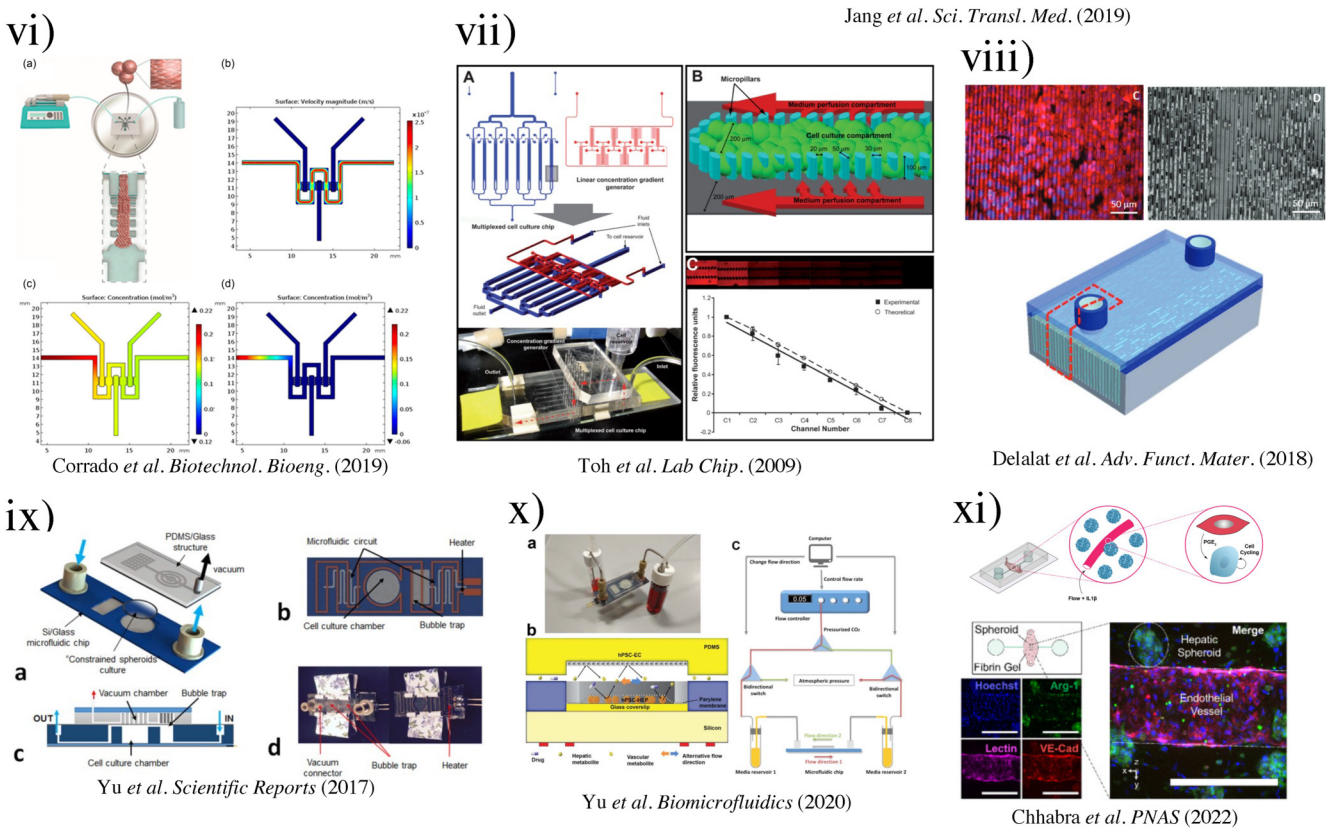

FIG. 6. (*Continued.*)

underlying cellular and molecular mechanisms of NAFLD pathogenesis and progression remain largely debatable and having LOCs which provide a reproducible and accurate disease model would accelerate discoveries of potential treatments.

To this front, Gori *et al.* followed the work of Lee *et al.* and designed LOCs with an augmented cell culture chamber.[99] HepG2/C3A cells (CRL-10741) were seeded, and subjected to fluid flow of 18 μl/day for 8 days through a gravity-operated mass transport channel [Fig. 6(iii)]. To induce steatosis, cells were treated with free fatty acids (FFAs), palmitic acid (PA; 16:0), and oleic acid (OA; 18:1 cis-9) in methanol. This model maintained higher hepatic cell viability and minimal oxidative stress compared to 2D static cultures. This was one of the first *in vitro* LOC models of human NAFLD in a sinusoid-like fashion.

To systematically study different microenvironmental conditions and their impacts on cell behavior in liver disease, single channeled LOCs presented above can become laborious and impractical. Bulutoglu *et al.* utilized a microfluidic gradient generator, shown in Fig. 6(iv), to create highly reproducible chemical gradients that allowed continuous media flow.[95] In this model, Metabolic Patterning on a Chip (MPOC) platform with the ability to generate five defined gradients of FFA concentrations was used. The platform was capable of inducing oxygen deprivation in incremental changes. Using rat primary hepatocytes, the oxygen gradient was shown to impose the highest effect on fat storage at the lowest FFA concentration. This LOC was useful for simulating a spectrum of disease progression, as well as aiding in dissecting the effects of spatial heterogeneity, which previous models have not been able to achieve.

B. Models for studying drug metabolism and nanotoxicity

LOCs have been developed to mimic the metabolic functions of the liver, for instance, the two phases of drug metabolism.[182] Phase I (non-synthetic) involves oxidation, reduction, hydrolysis, and hydroxylation, while Phase II (synthetic) is the conjugation with an endogenous ligand (e.g., glycine, glucuronide, glutathione, or sulfate).[183] When a drug undergoes metabolism in the liver, it could experience one of the two phases or a combination of the two. Phases I and II are performed mainly by hepatocytes. Cytochrome P450 (CYP) family enzymes from phase I and transferases from phase II could transform the insoluble toxic substances from phase I into less toxic and soluble substances.[184] Thus, the measurement of CYP could be a biomarker for high metabolic

activity of hepatocytes. Long-term hepatic cell culture is an important tool for studying drug metabolism *in vitro*. The use of a microfluidics device or perfusion-based device can collect and recirculate hepatic biomarkers, which was impossible to achieve using conventional methods. LOC platforms can help sustain the phenotype of hepatocytes and liver-specific functions in long-term culture.[130]

The primary cause of drug attrition in preclinical testing is drug-induced liver injury. For this reason, it is essential to develop a reliable, accurate and reproducible *in vitro* hepatic platform for predicting drug toxicity. The current method of characterizing absorption, distribution, metabolism, excretion, and toxicity of new drugs relies on animal models, which often fail to predict human responses due to species-specific differences in drug metabolism pathways.[185,186] As an example, a study led by the company Emulate [Fig. 6(v)][101] showed species-specific drug toxicity responses when modeled using a Liver-Chip, highlighting the need to use human primary cell lines in the model. The Emulate chip had an interesting design that could further benefit from incorporating organ-specific features. For instance, the membrane structure could have been replaced with other types of barrier structures, such as pillars, to encourage biliary structure formation. Another consideration was to vary the membrane pores sizes to simulate fenestrae structures as listed in Table III. Furthermore, an investigation of the changes in dimensionless numbers with different flow conditions and channel geometry designs could be beneficial to better understand the mechano-responses of liver cells *in vitro*.

In another study, Corrado *et al.* developed a LOC with HepG2 cell line that showed prolonged functional performance and capacity to be used as a predictive platform for studying the cytotoxic effects of xenobiotics and drugs [Fig. 6(vi)].[96] They evaluated the distribution of oxygen under a flow rate of 5 μl/min in the chip, showing close to 100% of oxygen equilibrium concentration (0.22 mol/m^3) in the first compartment with progressively lower percentage and the lowest at 55% (0.124 mol/m^3) in the final compartment. As a proof-of-concept study, ethanol (100 and 300 mM) was used to study alcoholic liver injury for 2 or 4 days. Through damage quantification (albumin and urea decreased production), the system was shown to be suitable for sensing hepatotoxicity.

A microfluidic 3D hepatocyte chip (3D HepaTox chip) with a different design was used to recapitulate *in vivo* liver functions for *in vitro* assessment of drug toxicity [Fig. 6(vii)].[187] Toh *et al.* designed this chip with eight parallel cell culture channels independently controlled by a concentration generator. Each cell culture channel was separated into three distinct compartments by an array of elliptical micropillars, with one central cell culture compartment and two side perfusion compartments. The HepaTox chip accurately predicted hepatotoxicity using five model drugs in a dose-dependent manner. The IC_{50} values obtained using this *in vitro* platform showed a positive correlation to *in vivo* experiments, suggesting its usefulness in drug testing and screening. However, the study also noted that the required volume of conventional assays for cytotoxicity testing exceeds the typical operating volume of the chip, and a highly sensitive micro-biosensor was needed to accurately reflect the IC_{50} value using this LOC.

In another interesting design, 3D heparin-coated microtrenches were produced to mimic the architecture of hepatic sinusoids [Fig. 6(viii)].[97] This design recapitulated 3D microarchitecture, cord-like arrangement of hepatocytes, and physiological microcirculation, with an optimal microtrench of 20 μm depth. This model was able to maintain cell viability and hepatocyte function over 4 weeks, verified by measuring basal levels of cytochrome P450 activity. The model also produced IC_{50} values for the model drugs acetaminophen, tacrine, and chlorpromazine in agreement with LD_{50} values *in vivo*, suggesting its capability for evaluating liver response to hepatotoxins.

A typical problem faced by OOCs including LOCs is air bubble contaminants, which could cause detrimental effects once they burst. Although a bubble trap can prevent large bubbles from entering the culture chamber, the accumulation of tiny bubbles or the formation of dissociated gas is difficult to suppress. To overcome this problem, Yu *et al.* created a perfusion-incubator-liver-chip (PIC), which maintained hepatic cell viability over 3 weeks and their functions over 2 weeks [Fig. 6(ix)].[110] The design criteria for this chip to be used in chronic liver toxicity testing were: organotypic 3D cellular architecture, good mass transfer, maintenance of mechanical forces and limited shear stress to the cells, stable cell culture conditions, and ease of handling cells and replenishing media. A hydrophilic surface of the microfluidic elements prevented rapid adsorption of proteins and drug molecules. The use of silicon structures with good thermal conductivity helped to maintain uniform media temperature. The PIC operated at an optimal flow rate of 0.1 ml/h, and showed higher sensitivity in evaluating chronic drug response to repeated dosing of diclofenac and acetaminophen compared to the static culture control.

To further improve the performance of the PIC, Yu *et al.* recirculated the culture media in a follow-up study to better predict drug toxicity due to the accumulation of metabolites in the solution [Fig. 6(x)].[109] The PIC was a parallel culturing chamber where the top had human pluripotent stem cells (hPSC)-derived vascular cells, and the bottom hPSC-derived hepatocyte spheroids. Better attachment of hPSC-derived endothelial cells was achieved by modifying the PDMS surface using 3,4-dihydroxy-L-phenylalanine (DOPA). This recirculating perfusion chip co-culturing system demonstrated superior performance over the conventional static culture platform.

LOCs have also found interesting applications in nanotoxicity evaluation as another type of metabolic study. The increasing use of nanomedicine therapeutics, such as mRNA vaccines, can undergo different routes of clearance depending on their (organic or inorganic) compositions.[188] Synthetic nanomaterials might introduce nanotoxicity during their clearance and biodegradation by the body, largely through the liver. For instance, nanoparticles (NPs) with a hydrodynamic diameter (HD) less than 5 nm are found to result in rapid renal clearance, but the same clearance mechanism is prohibited with NPs over 15 nm in HD.[189] New nanomedicine therapeutics have faced barriers to translation partly due to the potential of nanomaterials to trigger immune responses or accumulate in the mononuclear phagocyte system.[35–190] Currently, our knowledge of the long-term toxicity responses of new nanomaterials remain limited, giving rise to a growing concern about the health risks of using nanotherapeutics or medical implants that produce nanoparticles from wearing. Animal models do not always provide accurate or reliable prediction of human physiological response in the assessment of nanotoxicity due to inter-species differences.[22–191] lOCs could provide a solution

to fill this gap, which can be constructed with human cells for screening the safety of nanomedicine, and provide physiologically relevant data to predict *in vivo* behavior of nanomaterials as well as associated biological response.

In a recent study, Li *et al.* developed a 3D hepatocyte chip that recapitulated key physiological responses in the hepatotoxicity response of superparamagnetic iron oxide nanoparticles (SPION).[29] Rat hepatocytes were freshly isolated and used for tissue culture with collagen gel. Three-day (short-term) and one-week (long-term) liver-specific functions were evaluated in the presence of different doses of SPION. Analyses performed using the LOC suggested that cumulative exposure to nanoparticles resulted in more dramatic hepatocyte damage. Surface patterning is another technique that can be used to maintain long-term cell culture.[192] To evaluate the safety of silver nanoparticles (AgNPs), Liu *et al.* developed a LOC culturing system with patterned electrospun poly-DL-lactide fibers.[193] They investigated the impacts of flow rates on hepatocyte viability and found the optimal flow rate to be 10 μl/min, which was able to maintain cells for up to 15 days. Primary rat hepatocytes were cultured in the perfusion system and exposed to 120 μg/ml AgNPs for 24 h. The damage induced by AgNPs was assessed by measuring the activity of lactate dehydrogenase. The LOC system showed a higher sensitivity for measuring AgNPs induced toxicity compared to cells grown under static conditions. After treatment with AgNPs, 50% of cells died after 24 h, which was in agreement with the findings of Faedmaleki *et al.*, who reported an AgNPs IC_{50} value of 121.7 μg/ml in primary rat hepatocytes.[194] In these studies, LOCs provided a robust platform for investigating the hepatotoxicity profiles of nanomaterials, which could provide important data for their translation into clinical use.

C. Pharmacokinetic models

In recent developments, LOCs have been integrated with other OOC systems (e.g., gut, lung, kidney) to form microphysiological systems (MPS) for quantitatively analyzing and predicting human drug pharmacokinetics (PK) *in vitro*, specifically drug absorption, distribution, metabolism, and excretion (ADME). Compared to traditional animal models and cell cultures that often fail to correctly predict drug toxicity and efficacy due to inter-species differences,[195,196] MPS offers human multi-organ models with greater physiological relevance, yielding results that better match with human clinical data.[57–200] A multi-species (rat, dog, and human) LOC system has also been reported, where Jang *et al.* incorporated hepatocytes, sinusoidal endothelial cells, Kupffer cells, and hepatic stellate cells for predicting species-specific drug metabolism and toxicity.[101]

A recent study has found that the quantitative prediction of PK parameters for oral nicotine can be achieved by computational simulation of fluidically coupled gut, liver, and kidney organ chips with an arteriovenous reservoir for drug mixing.[198] The whole system is modeled as a set of ordinary differential equations (ODEs) that describe drug transport across different compartments. The general transport equation for the drug is defined as

$$\frac{\partial C}{\partial t} + \nabla(vC) = \nabla\,(D\nabla C) + S, \tag{2}$$

where C, D, v, and S denote the drug concentration, diffusion coefficient, fluid velocity, and the source term, respectively. Equation (2) is further derived into a set of fluxes equations for each model compartment,

$$V_B \frac{dC_B}{dt} = Q_B\,(C_{B,\,in} - C_B) + J_{B-M}\,, \tag{3}$$

$$V_M \frac{dC_M}{dt} = J_{M-A} - J_{B-M}\,, \tag{4}$$

$$V_A \frac{dC_A}{dt} = Q_A\,(C_{A,\,in} - C_A\,) + J_{M-A}\,, \tag{5}$$

where the subscripts B, M, and A refer to the basal channel, membrane, and apical channel, respectively. J represents the transmembrane diffusive fluxes and Q is the flow rate in the microchannels. The predicted maximum concentration of nicotine (0.050 μM) showed a close match with the clinically measured value in patient blood (0.052 μM). Moreover, this model showed a better fit to human PK parameters than ones measured from rodents.

In addition, a multi-organ model has been proposed that integrates seven organ-chips, including the brain, heart, pancreas, liver, lung, gut, and endometrium to study the PK parameters of diclofenac.[199] The predicted drug concentration using this model agreed with experimentally measured values. The reader is referred to a review on more multi-organ chip studies for PK of certain drugs.[201]

D. Multi-component sensing platforms

LOCs can be used in conjunction with sensors for real-time monitoring and analysis of *in vitro* hepatic responses. In one of the first studies in this area, Schober *et al.* incorporated biosensors in conjunction with LOC to study *in vitro* cell culture.[202] AlGaN/GaN nanosensors were used due to their high sensitivity, chemical stability, biocompatibility, and label-free detection. Albumin was used as the metabolic marker to compare the *in vitro* cultures and their *in vivo* counterparts. More recently, Zhang *et al.* constructed a platform for accurate drug screening using LOCs, seeded with Hep-G2 (liver cancer cells).[203] They incorporated a real-time monitoring system consisting of electrochemical impedance and near-infrared spectroscopy measurements over five days, which provided quick sensing of liver state turnover. The system maintained 100% viability of hepatocytes over seven days, and allowed continuous real-time sensing of responses to paracetamol during drug resistance testing. More sophisticated designs have been reported,[204–206] and practical guides on fabricating integrated sensors for LOCs are captured in a recent protocol.[207]

Oxygen concentration in LOCs is a critical parameter that should be monitored in most applications, important for regulating cellular behavior and influencing cell differentiation and function.[24–210] However, the enclosed nature of microfluidic chips makes monitoring oxygen concentration in the culture media difficult. Although open microfluidics can provide easy access to cultured cells, it also requires precise and reliable liquid pumping equipment.[208] Changes in oxygen tension above (hyperoxia) or below (hypoxia) the physiological level, or complete absence

(anoxia) need to be closely monitored and controlled. Moya *et al.* presented an integrated amperometric oxygen sensor in a LOC system using an ultrathin porous cell culture membrane, achieving *in situ* real-time oxygen monitoring of the cell culture chamber [Fig. 7(i)].[107] As proof of concept, three electrochemical dissolved oxygen (DO) sensors were integrated with the porous membrane of the LOC device (ExoLiver). In cultures of primary rat and human hepatocytes, the DO sensors could detect an oxygen gradient up to 17.5% and 32.5% for respective cell populations. This study also demonstrated the feasibility of inkjet printing in sensor fabrication for use with LOCs, which could be extended for applications in other OOCs.

Other metabolic biomarkers can be important to characterize using LOCs for mechanistic studies. For instance, there is a strong need for high-resolution real-time analysis of biochemical and metabolic activities of living cells in LOCs. Weltin *et al.* demonstrated the use of an electrochemical microsensor that achieved label-free, *in situ* and continuous measurement of lactate and oxygen levels from single human HepaRG (HPR116) hepatocyte spheroids [Fig. 7(ii)].[208] The lactate sensor was immobilized with lactate oxidase in a hydrogel matrix and showed a sensitivity up to 134 nA/mm^2. This design sustained up to 70 h of continuous metabolite monitoring. To further test the sensor performance, cells were exposed to antimycin A, which suppressed the aerobic metabolic pathway, and Bosentan, a dual endothelin receptor antagonist that could induce liver injury. Measurements showed clear dose-dependent metabolic behavior, confirming the ability of this LOC system for continuous monitoring of hepatocyte metabolism and toxicological applications.

In a similar approach, Shin *et al.* focused on monitoring albumin and GTS-α using electrochemical sensors [Fig. 7(iii)].[209] They developed on-chip valves to manipulate the fluid flow, and the ability to perform repeated measurements and surface cleaning cycles in an automated fashion using a WAGO controller. The metabolic activity of primary human hepatocyte spheroids was measured for up to 7 days. The limit of detection was 0.09 ng/ml for albumin and of 50 ng/ml for GTF-α. This could be a unique universal strategy for constructing automated microfluidic-based sensors for continuous monitoring of drug toxicity using OOCs.

Liver injury is a complicated process that involves secreted signaling molecules, such as cytokines and growth factors, which could be impractical to measure in co-cultured cells grown in conventional cell culture. LOCs can be designed to have actuating compartments for studying individual cell-secreted signaling molecules. Zhou *et al.* recently presented reconfigurable microfluidics integrated with a miniaturized aptamer-based biosensor [Fig. 7(iv)].[8] The LOC contained a pneumatic actuatable wall, which could be raised or lowered to create different device configurations. The reconfigurable compartments were used to co-culture primary rat hepatocytes with human stellate cells (LX2). This model revealed that alcohol injury would cause hepatocytes to secrete FGF-β molecules and trigger neighboring stellate cells to release more. Similar designs could be useful for studying other hepatic paracrine signals.

VI. SUMMARY AND FUTURE PERSPECTIVES

LOCs have provided new means for studying liver physiology, disease progression, and associated mechanisms, as well as been used in a variety of applications related to drug screening. With continuous developments in nanomedicine, LOCs are gaining increasing value as platforms for nanotoxicity studies to advance the translation of new nanotherapeutics. By providing a more physiologically relevant and cost-effective *in vitro* model of liver responses, LOCs may accelerate the progression of policymaking and approval of nanomedicine strategies.[211] Multi-chip LOC systems could further accelerate drug development and provide insights to a multi-organ or cross-species response, bringing immense economic benefits. It was estimated that the utility of OOCs, and especially LOCs in pharmaceutical industries and preclinical development could lead to a 26% reduction in research and development cost for new medical therapeutics.[212] Furthermore, OOC technology in general offers the hope to replace, reduce, and refine (the "3Rs") the use of animal models in research, which is particularly important for LOCs since the majority of studies relating to the liver are still performed using animal models. Nevertheless, many gaps and challenges remain.[5–213] Here, we provide further insights into potential future developments in LOCs for their broader applications.

A. Fit-for-purpose LOC model

Although multi-organ chips have been used in preclinical studies of drug development to test toxicity and PK *in vitro* (discussed in Sec. V E), one of their primary disadvantages is that such models need to be tuned to suit specific target drugs or species. This is time consuming and not cost-effective but can be potentially overcome by developing a unified OOC system that could be implemented in screening different drugs without redefining the overall modeling of the system.[105–214]

Li *et al.* developed an adaptable model of the liver acinus using a glass-based microfluidic device, which could be customized by tuning the shear stress and flow rate to optimize liver zonation.[105] Other efforts have been taken to mimic the architectural features of the liver organization and provide adaptable models that could potentially be incorporated into multi-organ chip systems.[215,216] However, further work is required to fully deliver a model that could accurately depict the portal triad, central vein, sinusoid, and bile canaliculi.

B. Recapitulation of liver heterogeneity

Zonal differences exhibit clinical significance in drug-induced liver injury.[217] Thus, the ability to recapitulate hepatic zonal physiology is critical for predicting drug toxicity using LOCs. Current models have not been able to fully capture complex and multifaceted hepatic physiology, especially in long-term culture. Drug-induced hepatotoxicity and zonal effects need to be studied using improved LOCs, for instance, using a modular system that couples biochemical and biophysical cues, and incorporates the essential roles of mechanical forces in cellular development and signal transduction.[218]

C. Mechanistic study of liver regeneration

The liver is unique as it is the only organ in the human body that has a high regenerative capacity and still performs complex

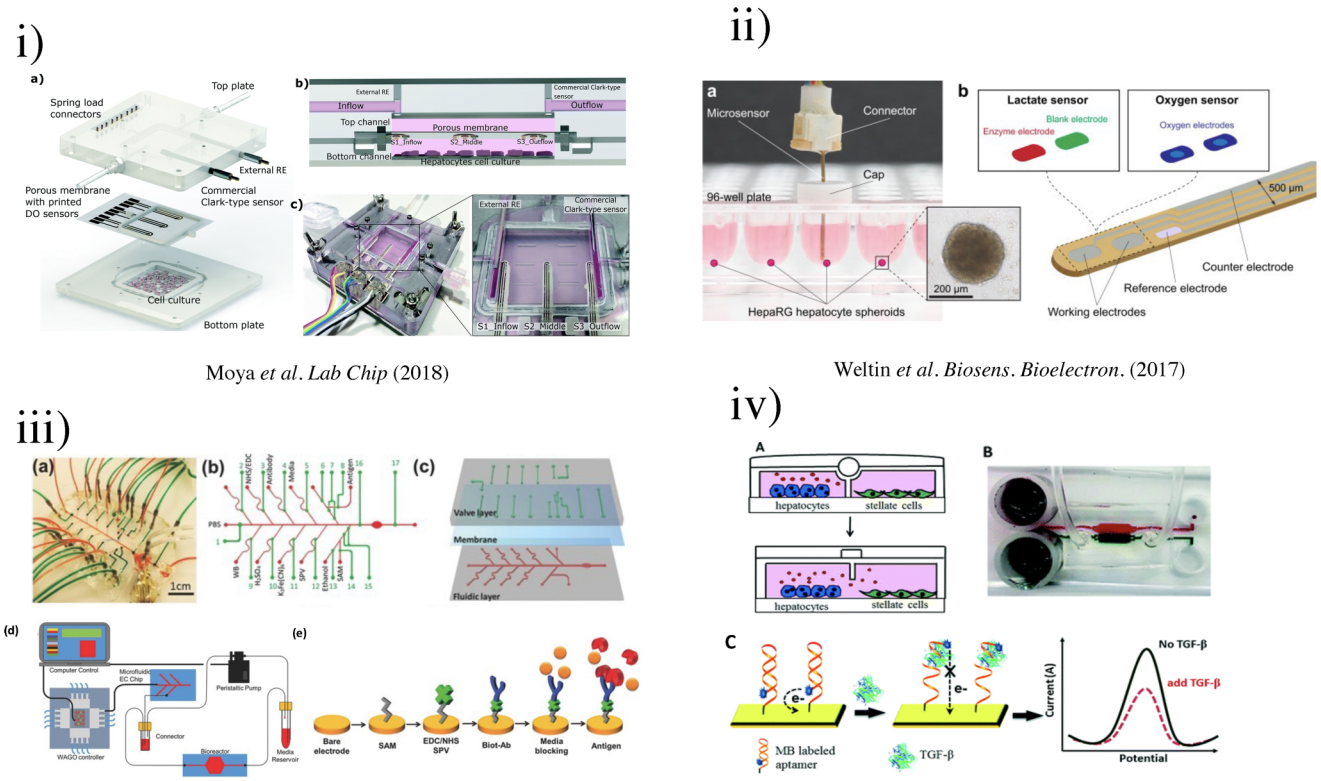

FIG. 7. (i) (a) Schematic of the OOC system with modifications to incorporate the control with external elements and the spring load for the connectors on the top plate, (b) cross section of the bioreactor showing the position of the three DO printed sensors, and (c) real picture of the ExoLiver system with all fluidic and electrical connections.[107] Reproduced with permission from Moya *et al.*, Lab Chip **18**(14), 2023–2035 (2018). Copyright 2018 the Royal Society of Chemistry. (ii) (a) Measurement setup with microsensor device placed in the 96-well cell culture plate. (b) Close-up scheme of microsensor tip with electrode layout.[208] Reproduced with permission from Weltin *et al.*, Biosens. Bioelectron. **87**, 941–948 (2017). Copyright 2016 Elsevier. (iii) Design, fabrication, and control of the automated microfluidic EC biosensor. (a) Photograph of the lectrochemical (EC) microfluidic chip bonded with a microelectrode. (b) Labeling of the microfluidic channels and the valves with corresponding flowing solutions for fully automated biosensing measurements. (c) Three-layered microfluidic chip consisting of the microfluidic channel, a thin membrane, and the valve channel layer. (d) Schematic of the microfluidic EC biosensing system integrated with organ-on-a-chip for continual monitoring of a target biomarker in an automated manner. (e) A schematic illustration for immobilization of antibodies using streptavidin on the surface of the microelectrodes.[209] Reproduced with permission from Shin *et al.*, Adv. Sci. (Weinh) **4**(5), 1600522 (2017). Copyright 2017 WILEY-VCH Verlag GmbH & Co. KGaA, Weinheim. (iv) (a) Design of reconfigurable microfluidic co-culture system. (b) A typical microfluidic device used in a co-culture experiment. The wall separating microchannels was lowered to demonstrate the food dye did not mix. (c) Principle of TGF-β detection. The binding of cytokine molecules causes aptamer molecules to change conformation.[8] Reproduced with permission from Zhou *et al.*, Lab Chip **15**(23), 4467–4478 (2015). Copyright 2015 the Royal Society of Chemistry.

functions. Loss of liver mass will trigger liver regeneration, which occurs in all vertebrate organisms from fish to mammals.[219] Stable liver function is critical for optimal brain function, otherwise leading to chronic "hepatic encephalopathy" and eventual coma.[220] The liver also dynamically responds to changes in physiological conditions by changing its size.[221] For example, the liver increases in size during pregnancy and decreases in size from severe loss in body weight.

To understand liver regeneration and these complex physiological processes using an *in vitro* model is inarguably difficult. Recently, Chhabra *et al.* designed LOCs which successfully mimicked hepatocyte regeneration, using a microfluidic model named structurally vascularized hepatic ensembles for analyzing regeneration (SHEAR).[57] SHEAR captured the flow-dependent paracrine aspects of human liver regeneration by linking a parenchymal compartment and a biomaterial lumen [Fig. 6(xi)]. The parenchymal compartment consisted of 3D spheroids composed of primary human hepatocytes and human dermal fibroblasts, while the lumen of the channel was embedded within an extracellular matrix and lined with human endothelial cells. Using this model, they identified IL-1β as a key molecule that could be responsible for initiating hepatocyte proliferation.

A few improvements may be made to the above model to more accurately capture physiological liver regeneration, such as (i) using natural ECM-derived biomaterials that better replicate liver physiological conditions; (ii) investigating the effects of fluid flow

on various pathways implicated in liver regeneration, as well as pathological changes involved in cirrhosis, and (iii) adding physical perturbation (e.g., heat) or hepatotoxins to the model for studying liver regeneration in response to injury.

D. Real-time biosensing

OOC devices have been coupled with a variety of biosensing approaches to track the temperature, pH, cell metabolism, and responses to the external environment. Apart from recent developments in LOC-integrated biosensing platforms discussed in Sec. V E, LOCs could also be used in multi-organ sensing systems for studying liver injury induced by factors such as environmental pollution or pesticides.[222,223] Additionally, OOC sensing systems have been used to perform long-term (28 days) monitoring of different cell functions.[224] A future goals for LOC sensing platforms would be to integrate multi-sensors with multi-organ chips to create a unified system for detecting various parameters such as metabolic indicators (e.g., oxygen concentration), physical activities (e.g., cardiac beating rates), and biomarkers, for *in vitro* drug screening and disease modeling. Since different types of sensors (electrical, electrochemical, and optical) are needed for monitoring different biochemical activities, the main challenge of such a system would be the miniaturization and integration of various biosensors into a single platform with minimal interference among them. The complexity of output data from a multi-sensor system could create obstacles in design, which might benefit from machine learning algorithms for data analysis.[225–227]

E. Human-on-a-chip systems

Human-on-a-chip refers to the total mimicry of human physiochemical responses using OOC technology, often considered the ultimate *in vitro* model for drug screening and disease studies.[228,229] The human body is intricate and functions through closely interconnected organ systems, with many organ functions being highly dependent on each other. Studying individual organs using *in vitro* models will not provide the same physiological relevance as a systematic model, which is the greatest shortcoming for OOC devices modeling specific organs compared to animal models. By incorporating LOC devices with other organs of interest, such as gut,[230] skin,[231] cardiac-muscle-neuronal,[232] pancreas,[233,234] lung,[24] and kidney,[235] human disease models could be more readily recapitulated through *in vitro* systems to produce highly relevant physiological data. The main advantage of connecting these MPS is that complicated modeling of drug absorption, distribution, metabolism and excretion (ADME) and physiological-based pharmacokinetics could be achieved,[236] ultimately serving as a predictive tool for drug development.[237] A prime example is the study by Sung and Shuler,[238] where a LOC device was fabricated to mimic multi-organ interactions by co-culturing liver cells (HepG2/C3A), tumor cells (HCT-116), and bone marrow cells (Kasumi-1) in separate chambers. The pharmacokinetic and pharmacodynamic profiles of the anticancer drug, Tegafur, were analyzed. This system was able to metabolize tegafur into its active component which led to cell death, proving the physiological relevance of such MPS platforms.

LOC devices may perform more accurately than animal models in toxicity assessment in the early stages of drug development, but it is currently impossible to entirely replace animal testing using isolated LOCs or those integrated into more complex multi-organ or human-on-a-chip systems. Nevertheless, LOCs have already exhibited potential to dramatically reduce the number of animals used in preclinical testing, particularly for drug toxicity assessment and preclinical screening.[200–239]

F. Numerical simulation and machine learning-aided design

In silico modeling of microfluidics devices by COMSOL has been widely used in designing microchannel geometries and investigating fluid behavior for achieving optimal performance.[240] Computational simulation can reduce the design cost and shorten the design cycle by virtually testing the system with a combination of parameters before actual fabrication.[241,242] In OOC devices, COMSOL has been used to analyze the impact of changes in microchannel dimensions and flow rate on the wall shear stress and fluid velocity, which may impact cell responses.[240] This software can be similarly utilized to quantitatively monitor the metabolic function of cells within LOC devices.[243] Building the 3D model in COMSOL and tuning the parameters to achieve the desired outcome can complement or validate the experimentally-obtained data.

Machine learning has taken off tremendously in recent years due to rapid advances in computing power, which could aid in creating intelligent structural designs of microfluidic chips.[244] For instance, machine learning could be used to validate microfluidic designs prior to fabrication, or used to calculate the required flow speed for the media to achieve physiologically relevant experimental conditions.[245–247] The adoption of machine learning into OOC design requires data training and collaboration across multiple fields, which hopefully in the future will inform desired model chip parameters such as the number of cells per channel, shear force on cells, cell density, and cell type.[248,249] Adapting existing algorithms to produce intelligent designs for OOCs or specifically LOCs could be an incredibly cost-effective approach to generate physiologically relevant models of organ function.[250] This could be an emerging strategy to create new LOC devices that may also contribute to the development of automated human-on-a-chip, enhancing the throughput of future drug development, disease studies, and personalized medicine at a low cost.

AUTHOR DECLARATIONS

Conflict of Interest

The authors have no conflicts to disclose.

Author Contributions

Zhenxu Yang: Conceptualization (equal); Formal analysis (equal); Methodology (equal); Project administration (equal); Validation (equal); Writing – original draft (lead); Writing – review & editing (equal). **Xiaochen Liu:** Conceptualization (supporting); Formal analysis (equal); Project administration (equal); Resources (supporting); Supervision (supporting); Validation (equal); Writing –

original draft (equal); Writing – review & editing (equal). **Elise M. Cribbin:** Formal analysis (supporting); Investigation (supporting); Validation (supporting); Writing – review & editing (supporting). **Alice M. Kim:** Formal analysis (supporting); Investigation (supporting); Validation (supporting); Writing – review & editing (supporting). **Jiao Jiao Li:** Conceptualization (supporting); Formal analysis (equal); Investigation (equal); Project administration (equal); Supervision (equal); Validation (equal); Writing – review & editing (equal). **Ken-Tye Yong:** Conceptualization (equal); Formal analysis (equal); Funding acquisition (equal); Project administration (equal); Resources (lead); Supervision (equal); Validation (equal); Visualization (equal); Writing – review & editing (equal).

DATA AVAILABILITY

Data sharing is not applicable to this article as no new data were created or analyzed in this study.

REFERENCES

[1]S. Breslin and L. O'Driscoll, Drug Discovery Today **18**(5), 240–249 (2013).
[2]P. Godoy, N. J. Hewitt, U. Albrecht, M. E. Andersen, N. Ansari, S. Bhattacharya, J. G. Bode, J. Bolleyn, C. Borner, J. Böttger, A. Braeuning, R. A. Budinsky, B. Burkhardt, N. R. Cameron, G. Camussi, C. S. Cho, Y. J. Choi, J. Craig Rowlands, U. Dahmen, G. Damm, O. Dirsch, M. T. Donato, J. Dong, S. Dooley, D. Drasdo, R. Eakins, K. S. Ferreira, V. Fonsato, J. Fraczek, R. Gebhardt, A. Gibson, M. Glanemann, C. E. P. Goldring, M. J. Gómez-Lechón, G. M. M. Groothuis, L. Gustavsson, C. Guyot, D. Hallifax, S. Hammad, A. Hayward, D. Häussinger, C. Hellerbrand, P. Hewitt, S. Hoehme, H. G. Holzhütter, J. B. Houston, J. Hrach, K. Ito, H. Jaeschke, V. Keitel, J. M. Kelm, B. Kevin Park, C. Kordes, G. A. Kullak-Ublick, E. L. Lecluyse, P. Lu, J. Luebke-Wheeler, A. Lutz, D. J. Maltman, M. Matz-Soja, P. McMullen, I. Merfort, S. Messner, C. Meyer, J. Mwinyi, D. J. Naisbitt, A. K. Nussler, P. Olinga, F. Pampaloni, J. Pi, L. Pluta, S. A. Przyborski, A. Ramachandran, V. Rogiers, C. Rowe, C. Schelcher, K. Schmich, M. Schwarz, B. Singh, E. H. K. Stelzer, B. Stieger, R. Stöber, Y. Sugiyama, C. Tetta, W. E. Thasler, T. Vanhaecke, M. Vinken, T. S. Weiss, A. Widera, C. G. Woods, J. J. Xu, K. M. Yarborough, and J. G. Hengstler, Arch. Toxicol. **87**, 1315–1530 (2013).
[3]C. Jensen and Y. Teng, Front. Mol. Biosci. **7**, 33 (2020).
[4]M. Kapałczyńska, T. Kolenda, W. Przybyła, M. Zajączkowska, A. Teresiak, V. Filas, M. Ibbs, R. Bliźniak, Ł Łuczewski, and K. Lamperska, Arch. Med. Sci. **14**(4), 910–919 (2018).
[5]C. Ma, Y. Peng, H. Li, and W. Chen, Trends Pharmacol. Sci. **42**(2), 119–133 (2021).
[6]S. S. Bale, L. Vernetti, N. Senutovitch, R. Jindal, M. Hegde, A. Gough, W. J. McCarty, A. Bakan, A. Bhushan, T. Y. Shun, I. Golberg, R. DeBiasio, O. B. Usta, D. L. Taylor, and M. L. Yarmush, Exp. Biol. Med. **239**(9), 1180–1191 (2014).
[7]J. H. Choi, L. Loarca, J. M. De Hoyos-Vega, N. Dadgar, K. Loutherback, V. H. Shah, G. Stybayeva, and A. Revzin, Am. J. Physiol.-Cell. Physiol. **319**(3), C552–C560 (2020).
[8]Q. Zhou, D. Patel, T. Kwa, A. Haque, Z. Matharu, G. Stybayeva, Y. Gao, A. M. Diehl, and A. Revzin, Lab Chip **15**(23), 4467–4478 (2015).
[9]D. Huh, B. D. Matthews, A. Mammoto, M. Montoya-Zavala, H. Y. Hsin, and D. E. Ingber, Science **328**(5986), 1662–1668 (2010).
[10]M. Kasendra, A. Tovaglieri, A. Sontheimer-Phelps, S. Jalili-Firoozinezhad, A. Bein, A. Chalkiadaki, W. Scholl, C. Zhang, H. Rickner, C. A. Richmond, H. Li, D. T. Breault, and D. E. Ingber, Sci. Rep. **8**(1), 2871 (2018).
[11]A. Bein, W. Shin, S. Jalili-Firoozinezhad, M. H. Park, A. Sontheimer-Phelps, A. Tovaglieri, A. Chalkiadaki, H. J. Kim, and D. E. Ingber, Cell. Mol. Gastroenterol. Hepatol. **5**(4), 659–668 (2018).
[12]M. A. Mofazzal Jahromi, A. Abdoli, M. Rahmanian, H. Bardania, M. Bayandori, S. M. Moosavi Basri, A. Kalbasi, A. R. Aref, M. Karimi, and M. R. Hamblin, Mol. Neurobiol. **56**(12), 8489–8512 (2019).
[13]A. Bhalerao, F. Sivandzade, S. R. Archie, E. A. Chowdhury, B. Noorani, and L. Cucullo, Fluids Barriers CNS **17**(1), 22 (2020).
[14]T.-E. Park, N. Mustafaoglu, A. Herland, R. Hasselkus, R. Mannix, E. A. FitzGerald, R. Prantil-Baun, A. Watters, O. Henry, M. Benz, H. Sanchez, H. J. McCrea, L. C. Goumnerova, H. W. Song, S. P. Palecek, E. Shusta, and D. E. Ingber, Nat. Commun. **10**(1), 2621 (2019).
[15]A. Herland, A. D. van der Meer, E. A. FitzGerald, T.-E. Park, J. J. F. Sleeboom, and D. E. Ingber, PLoS One **11**(3), e0150360 (2016).
[16]A. Skardal, S. V. Murphy, M. Devarasetty, I. Mead, H.-W. Kang, Y.-J. Seol, Y. Shrike Zhang, S.-R. Shin, L. Zhao, J. Aleman, A. R. Hall, T. D. Shupe, A. Kleensang, M. R. Dokmeci, S. Jin Lee, J. D. Jackson, J. J. Yoo, T. Hartung, A. Khademhosseini, S. Soker, C. E. Bishop, and A. Atala, Sci. Rep. **7**(1), 8837 (2017).
[17]B. M. Maoz, A. Herland, E. A. FitzGerald, T. Grevesse, C. Vidoudez, A. R. Pacheco, S. P. Sheehy, T. E. Park, S. Dauth, R. Mannix, N. Budnik, K. Shores, A. Cho, J. C. Nawroth, D. Segrè, B. Budnik, D. E. Ingber, and K. K. Parker, Nat. Biotechnol. **36**(9), 865–874 (2018).
[18]J. D. Caplin, N. G. Granados, M. R. James, R. Montazami, and N. Hashemi, *Advanced Healthcare Materials* (Wiley-VCH Verlag, 2015), Vol. 4, pp. 1426–1450.
[19]A. Saleh, R. DeBiasio, K. Wilschut, L. Vernetti, D. L. Taylor, P. Vulto, A. Gough, and A. Sharma, Drug Metab. Pharmacokinet. **34**(1), S50 (2019).
[20]A. A. Zakharyants, O. A. Burmistrova, and A. A. Poloznikov, Bull. Exp. Biol. Med. **162**(4), 515–519 (2017).
[21]A. D. Hingorani, V. Kuan, C. Finan, F. A. Kruger, A. Gaulton, S. Chopade, R. Sofat, R. J. MacAllister, J. P. Overington, H. Hemingway, S. Denaxas, D. Prieto, and J. P. Casas, Sci. Rep. **9**(1), 18911 (2019).
[22]M. B. Bracken, J. R. Soc. Med. **102**(3), 120–122 (2009).
[23]J. M. Wilkinson, *Organ-on-a-Chip* (Elsevier, 2020), pp. 1–11.
[24]D. Bovard, A. Sandoz, K. Luettich, S. Frentzel, A. Iskandar, D. Marescotti, K. Trivedi, E. Guedj, Q. Dutertre, M. C. Peitsch, and J. Hoeng, Lab Chip **18**(24), 3814–3829 (2018).
[25]J. Deng, Z. Chen, X. Zhang, Y. Luo, Z. Wu, Y. Lu, T. Liu, W. Zhao, and B. Lin, Biomed. Microdevices **21**(3), 57 (2019).
[26]J. Deng, W. Wei, Z. Chen, B. Lin, W. Zhao, Y. Luo, and X. Zhang, Micromachines (Basel) **10**(10), 676 (2019).
[27]D. J. Hughes, T. Kostrzewski, and E. L. Sceats, *Experimental Biology and Medicine* (SAGE Publications Inc., 2017), Vol. 242, pp. 1593–1604.
[28]K. K. Singh, *Patenting Nanomedicines: Legal Aspects, Intellectual Property and Grant Opportunities* (Springer-Verlag, Berlin, 2012), pp. 401–434.
[29]L. Li, K. Gokduman, A. Gokaltun, M. L. Yarmush, and O. B. Usta, Nanomedicine **14**(16), 2209–2226 (2019).
[30]S. Mvango, W. M. R. Matshe, A. O. Balogun, L. A. Pilcher, and M. O. Balogun, Pharm. Res. **35**(12), 237 (2018).
[31]K. Rahman, S. U. Khan, S. Fahad, M. X. Chang, A. Abbas, W. U. Khan, L. Rahman, Z. Ul Haq, G. Nabi, and D. Khan, Int. J. Nanomed. **14**, 1401–1410 (2019).
[32]S. Soares, J. Sousa, A. Pais, and C. Vitorino, Front. Chem. **6**, 360 (2018).
[33]R. Tenchov, R. Bird, A. E. Curtze, and Q. Zhou, ACS Nano **15**(11), 16982–17015 (2021).
[34]A. C. Anselmo and S. Mitragotri, Bioeng. Transl. Med. **4**(3), e10143 (2019).
[35]C. L. Ventola, Pharm. Ther. **42**(12), 742–755 (2017).
[36]A. A. Halwani, Pharmaceutics **14**(1), 106 (2022).
[37]G. H. Underhill and S. R. Khetani, Cell. Mol. Gastroenterol. Hepatol. **5**(3), 426–439.e1 (2018).
[38]S. Fowler, W. L. K. Chen, D. B. Duignan, A. Gupta, N. Hariparsad, J. R. Kenny, W. G. Lai, J. Liras, J. A. Phillips, and J. Gan, Lab Chip **20**(3), 446–467 (2020).
[39]C. M. Leung, P. de Haan, K. Ronaldson-Bouchard, G.-A. Kim, J. Ko, H. S. Rho, Z. Chen, P. Habibovic, N. L. Jeon, S. Takayama, M. L. Shuler, G. Vunjak-Novakovic, O. Frey, E. Verpoorte, and Y.-C. Toh, Nat. Rev. Methods Primers **2**(1), 33 (2022).

[40]A. J. Engler, S. Sen, H. L. Sweeney, and D. E. Discher, Cell **126**(4), 677–689 (2006).
[41]H. Gerardo, A. Lima, J. Carvalho, J. R. D. Ramos, S. Couceiro, R. D. M. Travasso, R. Pires das Neves, and M. Grãos, Sci. Rep. **9**(1), 9086 (2019).
[42]J. Friedrich, R. Ebner, and L. A. Kunz-Schughart, Int. J. Radiat. Biol. **83**(11–12), 849–871 (2007).
[43]J. W. Haycock, *Methods in Molecular Biology* (Humana Press, Clifton, NJ, 2011), Vol. 695, pp. 1–15.
[44]B. P. Chan and K. W. Leong, Eur. Spine J. **17**(Suppl 4), 467–479 (2008).
[45]Y. Zhang, D. Wu, X. Zhao, M. Pakvasa, A. B. Tucker, H. Luo, K. H. Qin, D. A. Hu, E. J. Wang, A. J. Li, M. Zhang, Y. Mao, M. Sabharwal, F. He, C. Niu, H. Wang, L. Huang, D. Shi, Q. Liu, N. Ni, K. Fu, C. Chen, W. Wagstaff, R. R. Reid, A. Athiviraham, S. Ho, M. J. Lee, K. Hynes, J. Strelzow, T. C. He, and M. El Dafrawy, Front. Bioeng. Biotechnol. **8**, 598607 (2020).
[46]R. Edmondson, J. J. Broglie, A. F. Adcock, and L. Yang, Assay Drug Dev. Technol. **12**(4), 207–218 (2014).
[47]M. Kozyra, I. Johansson, Å Nordling, S. Ullah, V. M. Lauschke, and M. Ingelman-Sundberg, Sci. Rep. **8**(1), 14297 (2018).
[48]A. Guillouzo, Environ. Health Perspect. **106**(Suppl 2), 511–532 (1998).
[49]M. Shulman and Y. Nahmias, in *Epithelial Cell Culture Protocols*, 2nd ed., edited by S. H. Randell and M. L. Fulcher (Humana Press, Totowa, NJ, 2013), pp. 287–302.
[50]P. Godoy, N. J. Hewitt, U. Albrecht, M. E. Andersen, N. Ansari, S. Bhattacharya, J. G. Bode, J. Bolleyn, C. Borner, J. Böttger, A. Braeuning, R. A. Budinsky, B. Burkhardt, N. R. Cameron, G. Camussi, C. S. Cho, Y. J. Choi, J. Craig Rowlands, U. Dahmen, G. Damm, O. Dirsch, M. T. Donato, J. Dong, S. Dooley, D. Drasdo, R. Eakins, K. S. Ferreira, V. Fonsato, J. Fraczek, R. Gebhardt, A. Gibson, M. Glanemann, C. E. Goldring, M. J. Gómez-Lechón, G. M. Groothuis, L. Gustavsson, C. Guyot, D. Hallifax, S. Hammad, A. Hayward, D. Häussinger, C. Hellerbrand, P. Hewitt, S. Hoehme, H. G. Holzhütter, J. B. Houston, J. Hrach, K. Ito, H. Jaeschke, V. Keitel, J. M. Kelm, B. Kevin Park, C. Kordes, G. A. Kullak-Ublick, E. L. LeCluyse, P. Lu, J. Luebke-Wheeler, A. Lutz, D. J. Maltman, M. Matz-Soja, P. McMullen, I. Merfort, S. Messner, C. Meyer, J. Mwinyi, D. J. Naisbitt, A. K. Nussler, P. Olinga, F. Pampaloni, J. Pi, L. Pluta, S. A. Przyborski, A. Ramachandran, V. Rogiers, C. Rowe, C. Schelcher, K. Schmich, M. Schwarz, B. Singh, E. H. Stelzer, B. Stieger, R. Stöber, Y. Sugiyama, C. Tetta, W. E. Thasler, T. Vanhaecke, M. Vinken, T. S. Weiss, A. Widera, C. G. Woods, J. J. Xu, K. M. Yarborough, and J. G. Hengstler, Arch. Toxicol. **87**(8), 1315–1530 (2013).
[51]E. L. LeCluyse, R. P. Witek, M. E. Andersen, and M. J. Powers, *Critical Reviews in Toxicology* (Taylor & Francis, 2012), Vol. 42, pp. 501–548.
[52]P. J. Lee, P. J. Hung, and L. P. Lee, Biotechnol. Bioeng. **97**(5), 1340–1346 (2007).
[53]H. Lee, W. Han, H. Kim, D.-H. Ha, J. Jang, B. S. Kim, and D.-W. Cho, Biomacromolecules **18**(4), 1229–1237 (2017).
[54]A. A. Banaeiyan, J. Theobald, J. Paukstyte, S. Wolfl, C. B. Adiels, and M. Goksor, Biofabrication **9**(1), 015014 (2017).
[55]S. Hassan, S. Sebastian, S. Maharjan, A. Lesha, A. M. Carpenter, X. Liu, X. Xie, C. Livermore, Y. S. Zhang, and A. Zarrinpar, *Hepatology* (John Wiley and Sons Inc., 2020), Vol. 71, pp. 733–740.
[56]Y. B. A. Kang, T. R. Sodunke, J. Lamontagne, J. Cirillo, C. Rajiv, M. J. Bouchard, and M. Noh, Biotechnol. Bioeng. **112**, 2571–2582 (2015).
[57]A. Chhabra, H.-H. G. Song, K. A. Grzelak, W. J. Polacheck, H. E. Fleming, C. S. Chen, and S. N. Bhatia, Proc. Natl. Acad. Sci. U.S.A. **119**(28), e2115867119 (2022).
[58]C. Horejs, Nat. Rev. Mater. **6**(5), 372–373 (2021).
[59]I. Dickson, *Nature Reviews Gastroenterology and Hepatology* (Nature Research, 2020), Vol. 17, p. 4.
[60]D. Huh, D. C. Leslie, B. D. Matthews, J. P. Fraser, S. Jurek, G. A. Hamilton, K. S. Thorneloe, M. A. McAlexander, and D. E. Ingber, Sci. Transl. Med. **4**(159), 159ra147 (2012).
[61]D. A. Ferreira, M. Rothbauer, J. P. Conde, P. Ertl, C. Oliveira, and P. L. Granja, Adv. Sci. **8**(8), 2003273 (2021).
[62]E. Ergir, B. Bachmann, H. Redl, G. Forte, and P. Ertl, Front. Physiol. **9**, 1417 (2018).
[63]B. K. Walther, N. K. Rajeeva Pandian, K. A. Gold, E. S. Kiliç, V. Sama, J. Gu, A. K. Gaharwar, A. Guiseppi-Elie, J. P. Cooke, and A. Jain, Lab Chip **21**(9), 1738–1751 (2021).
[64]C. L. Thompson, S. Fu, M. M. Knight, and S. D. Thorpe, Front. Bioeng. Biotechnol. **8**, 602646 (2020).
[65]S. S. Bale, S. Geerts, R. Jindal, and M. L. Yarmush, Sci. Rep. **6**(1), 25329 (2016).
[66]T. D. Troutman, H. Bennett, M. Sakai, J. S. Seidman, S. Heinz, and C. K. Glass, STAR Protoc. **2**(1), 100363 (2021).
[67]J. Deng, Y. Cong, X. Han, W. Wei, Y. Lu, T. Liu, W. Zhao, B. Lin, Y. Luo, and X. Zhang, Biomicrofluidics **14**(6), 064107 (2020).
[68]D. C. Duffy, J. C. McDonald, O. J. A. Schueller, and G. M. Whitesides, Anal. Chem. **70**(23), 4974–4984 (1998).
[69]Y. Nakao, H. Kimura, Y. Sakai, and T. Fujii, Biomicrofluidics **5**(2), 022212 (2011).
[70]J. Lee, S. H. Kim, Y. C. Kim, I. Choi, and J. H. Sung, Enzyme Microb. Technol. **53**(3), 159–164 (2013).
[71]S.-A. Lee, D. Y. No, E. Kang, J. Ju, D.-S. Kim, and S.-H. Lee, Lab Chip **13**(18), 3529–3537 (2013).
[72]Y. B. A. Kang, T. R. Sodunke, J. Lamontagne, J. Cirillo, C. Rajiv, M. J. Bouchard, and M. Noh, Biotechnol. Bioeng. **112**(12), 2571–2582 (2015).
[73]N. S. Bhise, V. Manoharan, S. Massa, A. Tamayol, M. Ghaderi, M. Miscuglio, Q. Lang, Y. Shrike Zhang, S. R. Shin, G. Calzone, N. Annabi, T. D. Shupe, C. E. Bishop, A. Atala, M. R. Dokmeci, and A. Khademhosseini, Biofabrication **8**(1), 014101 (2016).
[74]Y. S. Weng, S. F. Chang, M. C. Shih, S. H. Tseng, and C. H. Lai, Adv. Mater. **29**(36), 1701545 (2017).
[75]P.-Y. Chen, M.-J. Hsieh, Y.-H. Liao, Y.-C. Lin, and Y.-T. Hou, Biochem. Eng. J. **165**, 107831 (2021).
[76]M. Engel, L. Belfiore, B. Aghaei, and M. Sutija, SLAS Technol. **27**(1), 32–38 (2022).
[77]H. Wang, X. Liang, G. Gravot, C. A. Thorling, D. H. G. Crawford, Z. P. Xu, X. Liu, and M. S. Roberts, J. Biophotonics **10**(1), 46–60 (2017).
[78]E. N. Marieb and K. Hoehn, *Human Anatomy & Physiology* (Pearson Education, 2007).
[79]H. A. Stone and S. Kim, AIChE J. **47**(6), 1250–1254 (2001).
[80]V. S. Shirure and S. C. George, Lab Chip **17**(4), 681–690 (2017).
[81]J. H. Sung, Y. I. Wang, J. H. Kim, J. M. Lee, and M. L. Shuler, AIChE J. **64**(12), 4351–4360 (2018).
[82]Z. Kmieć, *Cooperation of Liver Cells in Health and Disease* (Springer, 2001), pp. 1–6.
[83]S. Guandalini, A. Dhawan, and D. Branski, *Textbook of Pediatric Gastroenterology, Hepatology and Nutrition* (Springer, 2016).
[84]I. M. Arias, H. J. Alter, J. L. Boyer, D. E. Cohen, D. A. Shafritz, S. S. Thorgeirsson, and A. W. Wolkoff, *The Liver: Biology and Pathobiology* (John Wiley & Sons, 2020).
[85]A. L. Mescher, *Junqueira's Basic Histology: Text and Atlas*, 13th ed. (McGraw-Hill Medical, New York, 2013).
[86]X. Ma, X. Qu, W. Zhu, Y.-S. Li, S. Yuan, H. Zhang, J. Liu, P. Wang, E. Lai Cheuk Sun, F. Zanella, G.-S. Feng, F. Sheikh, S. Chien, and S. Chen, Proc. Natl. Acad. Sci. U.S.A. **113**(8), 2206–2211 (2016).
[87]F. W. B. Sanders and J. L. Griffin, Biol. Rev. **91**(2), 452–468 (2016).
[88]T. Kietzmann, *Redox Biology* (Elsevier B.V., 2017), Vol. 11, pp. 622–630.
[89]C. Ma, L. Zhao, E.-M. Zhou, J. Xu, S. Shen, and J. Wang, Anal. Chem. **88**(3), 1719–1727 (2016).
[90]M.-C. Shih, S.-H. Tseng, Y.-S. Weng, I. M. Chu, and C.-H. Liu, Biomed. Microdevices **15**(5), 767–780 (2013).
[91]K. Rennert, S. Steinborn, M. Gröger, B. Ungerböck, A. M. Jank, J. Ehgartner, S. Nietzsche, J. Dinger, M. Kiehntopf, H. Funke, F. T. Peters, A. Lupp, C. Gärtner, T. Mayr, M. Bauer, O. Huber, and A. S. Mosig, Biomaterials **71**, 119–131 (2015).
[92]Y. Chen, W. Sun, L. Kang, Y. Wang, M. Zhang, H. Zhang, and P. Hu, Analyst **144**(14), 4233–4240 (2019).

[93]F. Bonanini, D. Kurek, S. Previdi, A. Nicolas, D. Hendriks, S. de Ruiter, M. Meyer, M. Clapes Cabrer, R. Dinkelberg, S. B. Garcia, B. Kramer, T. Olivier, H. Hu, C. Lopez-Iglesias, F. Schavemaker, E. Walinga, D. Dutta, K. Queiroz, K. Domansky, B. Ronden, J. Joore, H. L. Lanz, P. J. Peters, S. J. Trietsch, H. Clevers, and P. Vulto, Angiogenesis **25**(4), 455–470 (2022).
[94]J. A. Boos, P. M. Misun, A. Michlmayr, A. Hierlemann, and O. Frey, Adv. Sci. (Weinh) **6**(13), 1900294 (2019).
[95]B. Bulutoglu, C. Rey-Bedón, Y. B. Kang, S. Mert, M. L. Yarmush, and O. B. Usta, Lab Chip **19**(18), 3022–3031 (2019).
[96]B. Corrado, V. De Gregorio, G. Imparato, C. Attanasio, F. Urciuolo, and P. A. Netti, Biotechnol. Bioeng. **116**(5), 1152–1163 (2019).
[97]B. Delalat, C. Cozzi, S. Rasi Ghaemi, G. Polito, F. H. Kriel, T. D. Michl, F. J. Harding, C. Priest, G. Barillaro, and N. H. Voelcker, Adv. Funct. Mater. **28**(28), 1801825 (2018).
[98]O. Frey, P. M. Misun, D. A. Fluri, J. G. Hengstler, and A. Hierlemann, Nat. Commun. **5**(1), 4250 (2014).
[99]M. Gori, M. C. Simonelli, S. M. Giannitelli, L. Businaro, M. Trombetta, and A. Rainer, PLoS One **11**(7), e0159729 (2016).
[100]M. Jang, P. Neuzil, T. Volk, A. Manz, and A. Kleber, Biomicrofluidics **9**(3), 034113 (2015).
[101]K. J. Jang, M. A. Otieno, J. Ronxhi, H. K. Lim, L. Ewart, K. R. Kodella, D. B. Petropolis, G. Kulkarni, J. E. Rubins, D. Conegliano, J. Nawroth, D. Simic, W. Lam, M. Singer, E. Barale, B. Singh, M. Sonee, A. J. Streeter, C. Manthey, B. Jones, A. Srivastava, L. C. Andersson, D. Williams, H. Park, R. Barrile, J. Sliz, A. Herland, S. Haney, K. Karalis, D. E. Ingber, and G. A. Hamilton, Sci. Transl. Med. **11**(517), eaax5516 (2019).
[102]S. R. Khetani and S. N. Bhatia, Nat. Biotechnol. **26**(1), 120–126 (2008).
[103]Y. S. Kim, A. Asif, A. R. Chethikkattuveli Salih, J. W. Lee, K. N. Hyun, and K. H. Choi, Biomedicines **9**(10), 1369 (2021).
[104]H. Lee, S. Chae, J. Y. Kim, W. Han, J. Kim, Y. Choi, and D. W. Cho, Biofabrication **11**(2), 025001 (2019).
[105]X. Li, S. M. George, L. Vernetti, A. H. Gough, and D. L. Taylor, Lab Chip **18**(17), 2614–2631 (2018).
[106]E. Mazari-Arrighi, T. Okitsu, H. Teramae, H. Aoyagi, M. Kiyosawa, M. Yano, F. Chatelain, A. Fuchs, and S. Takeuchi, Sci. Rep. **12**(1), 1–12 (2022).
[107]A. Moya, M. Ortega-Ribera, X. Guimerà, E. Sowade, M. Zea, X. Illa, E. Ramon, R. Villa, J. Gracia-Sancho, and G. Gabriel, Lab Chip **18**(14), 2023–2035 (2018).
[108]A. D. Roth, P. Lama, S. Dunn, S. Hong, and M. Y. Lee, Mater. Sci. Eng. C **90**, 634–644 (2018).
[109]F. Yu, Y. T. Goh, H. Li, N. B. Chakrapani, M. Ni, G. L. Xu, T. M. Hsieh, Y. C. Toh, C. Cheung, C. Iliescu, and H. Yu, Biomicrofluidics **14**(3), 034108 (2020).
[110]F. Yu, R. Deng, W. Hao Tong, L. Huan, N. Chan Way, A. IslamBadhan, C. Iliescu, and H. Yu, Sci. Rep. **7**(1), 14528 (2017).
[111]W. F. Boron and E. Boulpaep, *Medical Physiology: A Cellular and Molecular Approach*, updated 2nd ed. (Elsevier Saunders, Philadelphia, PA, 2009).
[112]W. Pawlina and M. H. Ross, *Histology: A Text and Atlas: With Correlated Cell and Molecular Biology* (Lippincott Williams & Wilkins, 2018).
[113]X. Fu, J. P. Sluka, S. G. Clendenon, K. W. Dunn, Z. Wang, J. E. Klaunig, and J. A. Glazier, PLoS One **13**(9), e0198060 (2018).
[114]E. Wisse, J. Ultrastruct. Res. **31**(1–2), 125–150 (1970).
[115]K. Ogawa, T. Minase, K. Enomoto, and T. Onoé, Tohoku J. Exp. Med. **110**(1), 89–101 (1973).
[116]J. J. Widmann, R. S. Cotran, and H. D. Fahimi, J. Cell Biol. **52**(1), 159–170 (1972).
[117]F. Braet and E. Wisse, Comp. Hepatol. **1**(1), 1 (2002).
[118]E. Wisse, F. Jacobs, B. Topal, P. Frederik, and B. De Geest, Gene Ther. **15**(17), 1193–1199 (2008).
[119]R. Gebhardt, Pharmacol. Ther. **53**(3), 275–354 (1992).
[120]E. Wisse, R. B. de Zanger, K. Charels, P. van der Smissen, and R. S. McCuskey, Hepatology **5**(4), 683–692 (1985).
[121]T. Horn, P. Christoffersen, and J. H. Henriksen, Hepatology **7**(1), 77–82 (1987).
[122]B. Zapotoczny, K. Szafranska, K. Owczarczyk, E. Kus, S. Chlopicki, and M. Szymonski, Sci. Rep. **7**(1), 7994 (2017).
[123]K. Jungermann and D. Sasse, Trends Biochem. Sci. **3**(3), 198–202 (1978).
[124]N. Katz, H. F. Teutsch, K. Jungermann, and D. Sasse, FEBS Lett. **69**(1), 23–26 (1976).
[125]D. Sasse, N. Katz, and K. Jungermann, FEBS Lett. **57**(1), 83–88 (1975).
[126]W. G. Guder and U. Schmidt, Hoppe Seylers Z. Physiol. Chem. **357**(12), 1793–1800 (1976).
[127]D. Huh, H. J. Kim, J. P. Fraser, D. E. Shea, M. Khan, A. Bahinski, G. A. Hamilton, and D. E. Ingber, Nat. Protoc. **8**(11), 2135–2157 (2013).
[128]D. Bavli, S. Prill, E. Ezra, G. Levy, M. Cohen, M. Vinken, J. Vanfleteren, M. Jaeger, and Y. Nahmias, Proc. Natl. Acad. Sci. U.S.A. **113**(16), E2231–E2240 (2016).
[129]H. M. U. Farooqi, M. A. U. Khalid, K. H. Kim, S. R. Lee, and K. H. Choi, J. Micromech. Microeng. **30**(11), 115013 (2020).
[130]J. Zhang, X. Zhao, L. Liang, J. Li, U. Demirci, and S. Q. Wang, *Biomaterials* (Elsevier Ltd, 2018), Vol. 157, pp. 161–176.
[131]N. Kojima, F. Tao, H. Mihara, and S. Aoki, in *Stem Cells and Cancer in Hepatology*, edited by Y.-W. Zheng (Academic Press, 2018), pp. 145–158.
[132]M. Rothbauer, C. Eilenberger, S. Spitz, B. E. M. Bachmann, S. R. A. Kratz, E. I. Reihs, R. Windhager, S. Toegel, and P. Ertl, Front. Bioeng. Biotechnol. **10**, 837087 (2022).
[133]S. Hosic, A. J. Bindas, M. L. Puzan, W. Lake, J. R. Soucy, F. Zhou, R. A. Koppes, D. T. Breault, S. K. Murthy, and A. N. Koppes, ACS Biomater. Sci. Eng. **7**(7), 2949–2963 (2021).
[134]S. R. A. Kratz, C. Eilenberger, P. Schuller, B. Bachmann, S. Spitz, P. Ertl, and M. Rothbauer, Sci. Rep. **9**(1), 9287 (2019).
[135]Q. Li, K. Niu, D. Wang, L. Xuan, and X. Wang, Lab Chip **22**(14), 2682–2694 (2022).
[136]R. H. French and H. V. Tran, Annu. Rev. Mater. Res. **39**(1), 93–126 (2009).
[137]S. Rizvi, *Handbook of Photomask Manufacturing Technology* (CRC Press, 2018).
[138]R. Jose Varghese, E. h. M. Sakho, S. Parani, S. Thomas, O. S. Oluwafemi, and J. Wu, in *Nanomaterials for Solar Cell Applications*, edited by S. Thomas, E. H. M. Sakho, N. Kalarikkal, S. O. Oluwafemi, and J. Wu (Elsevier, 2019), pp. 75–95.
[139]D. G. Kasi, M. N. S. de Graaf, P. A. Motreuil-Ragot, J.-P. M. S. Frimat, M. D. Ferrari, P. M. Sarro, M. Mastrangeli, A. M. J. M. van den Maagdenberg, C. L. Mummery, and V. V. Orlova, Micromachines **13**(1), 49 (2022).
[140]G. G. Morbioli, N. C. Speller, and A. M. Stockton, Anal. Chim. Acta **1135**, 150–174 (2020).
[141]D. Qin, Y. Xia, and G. M. Whitesides, Nat. Protoc. **5**(3), 491–502 (2010).
[142]Y. Xia and G. M. Whitesides, Angew Chem. Int. Ed. Engl. **37**(5), 550–575 (1998).
[143]J. C. McDonald and G. M. Whitesides, Acc. Chem. Res. **35**(7), 491–499 (2002).
[144]S. B. Campbell, Q. Wu, J. Yazbeck, C. Liu, S. Okhovatian, and M. Radisic, ACS Biomater. Sci. Eng. **7**(7), 2880–2899 (2021).
[145]J. B. Nielsen, R. L. Hanson, H. M. Almughamsi, C. Pang, T. R. Fish, and A. T. Woolley, Anal. Chem. **92**(1), 150–168 (2020).
[146]S. M. Scott and Z. Ali, Micromachines **12**(3), 319 (2021).
[147]A. E. Danku, E. H. Dulf, C. Braicu, A. Jurj, and I. Berindan-Neagoe, Front. Bioeng. Biotechnol. **10**, 840674 (2022).
[148]Q. Wu, J. Liu, X. Wang, L. Feng, J. Wu, X. Zhu, W. Wen, and X. Gong, BioMed. Eng. OnLine **19**(1), 9 (2020).
[149]J. Friedrich, C. Seidel, R. Ebner, and L. A. Kunz-Schughart, Nat. Protoc. **4**(3), 309–324 (2009).
[150]N. Azizipour, R. Avazpour, M. Sawan, D. H. Rosenzweig, and A. Ajji, Sens. Diagn. **1**(4), 750–764 (2022).
[151]E. C. Costa, D. de Melo-Diogo, A. F. Moreira, M. P. Carvalho, and I. J. Correia, Biotechnol. J. **13**(1), 1700417 (2018).
[152]K. Moshksayan, N. Kashaninejad, M. E. Warkiani, J. G. Lock, H. Moghadas, B. Firoozabadi, M. S. Saidi, and N.-T. Nguyen, Sens. Actuators, B **263**, 151–176 (2018).

[153]R. M. Tostões, S. B. Leite, M. Serra, J. Jensen, P. Björquist, M. J. Carrondo, C. Brito, and P. M. Alves, Hepatology **55**(4), 1227–1236 (2012).
[154]E. Ferrari, G. S. Ugolini, C. Piutti, S. Marzorati, and M. Rasponi, Biomed. Mater. **16**(4), 045032 (2021).
[155]F. Behroozi, Phys. Teach. **60**(5), 358–361 (2022).
[156]D. Liu, S. Chen, and M. Win Naing, Biotechnol. Bioeng. **118**(2), 542–554 (2021).
[157]X. Wang and P. Yang, J. Vis. Exp. **17**, e825 (2008).
[158]B. Pinto, A. C. Henriques, P. M. A. Silva, and H. Bousbaa, *Pharmaceutics* (MDPI, 2020), Vol. 12.
[159]C. Chao, L. P. Ngo, and B. P. Engelward, ACS Biomater. Sci. Eng. **6**(4), 2427–2439 (2020).
[160]C. C. Bell, D. F. G. Hendriks, S. M. L. Moro, E. Ellis, J. Walsh, A. Renblom, L. Fredriksson Puigvert, A. C. A. Dankers, F. Jacobs, J. Snoeys, R. L. Sison-Young, R. E. Jenkins, Å Nordling, S. Mkrtchian, B. K. Park, N. R. Kitteringham, C. E. P. Goldring, V. M. Lauschke, and M. Ingelman-Sundberg, Sci. Rep. **6**(1), 25187 (2016).
[161]I. M. El-Sherbiny and M. H. Yacoub, Global Cardiol. Sci. Pract. **2013**(3), 316–342 (2013).
[162]S. Mantha, S. Pillai, P. Khayambashi, A. Upadhyay, Y. Zhang, O. Tao, H. M. Pham, and S. D. Tran, Materials (Basel) **12**(20), 3323 (2019).
[163]M. Ali and S. L. Payne, Biomater. Res. **25**(1), 5 (2021).
[164]J. van de Kamp, W. Jahnen-Dechent, B. Rath, R. Knuechel, and S. Neuss, Stem Cells Int. **2013**, 1 (2013).
[165]R. P. Bual and H. Ijima, Regen. Ther. **11**, 258–268 (2019).
[166]R. Grant, J. Hallett, S. Forbes, D. Hay, and A. Callanan, Sci. Rep. **9**(1), 6293 (2019).
[167]K. H. Hussein, K.-M. Park, L. Yu, H.-H. Kwak, and H.-M. Woo, Mater. Sci. Eng. C **116**, 111160 (2020).
[168]H. Shimoda, H. Yagi, H. Higashi, K. Tajima, K. Kuroda, Y. Abe, M. Kitago, M. Shinoda, and Y. Kitagawa, Sci. Rep. **9**(1), 12543 (2019).
[169]J. Wang, C. Shao, Y. Wang, L. Sun, and Y. Zhao, Engineering **6**(11), 1244–1257 (2020).
[170]A. K. Miri, E. Mostafavi, D. Khorsandi, S. K. Hu, M. Malpica, and A. Khademhosseini, Biofabrication **11**(4), 042002 (2019).
[171]K. Thakare, L. Jerpseth, Z. Pei, A. Elwany, F. Quek, and H. Qin, J. Manuf. Mater. Process. **5**(3), 91 (2021).
[172]S. Vijayavenkataraman, W. C. Yan, W. F. Lu, C. H. Wang, and J. Y. H. Fuh, Adv. Drug Delivery Rev. **132**, 296–332 (2018).
[173]S. V. Murphy and A. Atala, Nat. Biotechnol. **32**(8), 773–785 (2014).
[174]N. Ashammakhi, S. Ahadian, C. Xu, H. Montazerian, H. Ko, R. Nasiri, N. Barros, and A. Khademhosseini, Mater. Today Bio **1**, 100008 (2019).
[175]J. Hoeng, D. Bovard, and M. Peitsch, *Organ-on-a-Chip: Engineered Microenvironments for Safety and Efficacy Testing* (Academic Press, 2019).
[176]G. Janani, S. Priya, S. Dey, and B. B. Mandal, ACS Appl. Mater. Interfaces **14**(8), 10167–10186 (2022).
[177]T. Lyden, H. Hultgren, N. Beethe, R. Jaskens, M. LeBeau, and L. Thrun, FASEB J. **36**, 1 (2022).
[178]R. P. Evens, AAPS J. **18**(1), 281–285 (2016).
[179]D. Sun, W. Gao, H. Hu, and S. Zhou, Acta Pharm. Sin. B **12**(7), 3049–3062 (2022).
[180]E. M. Brunt, V. W. S. Wong, V. Nobili, C. P. Day, S. Sookoian, J. J. Maher, E. Bugianesi, C. B. Sirlin, B. A. Neuschwander-Tetri, and M. E. Rinella, Nat. Rev. Dis. Primers **1**(1), 15080 (2015).
[181]S. Klein and J. F. Dufour, Hepatic Oncol. **4**(3), 83–98 (2017).
[182]O. A. Almazroo, M. K. Miah, and R. Venkataramanan, Clin. Liver Dis. **21**(1), 1–20 (2017).
[183]K. Marcdante and R. M. Kliegman, *Nelson Essentials of Pediatrics, e-Book* (Elsevier Health Sciences, 2014).
[184]R. Gebhardt, J. G. Hengstler, D. Müller, R. Glöckner, P. Buenning, B. Laube, E. Schmelzer, M. Ullrich, D. Utesch, N. Hewitt, M. Ringel, B. R. Hilz, A. Bader, A. Langsch, T. Koose, H.-J. Burger, J. Maas, and F. Oesch, Drug Metab. Rev. **35**(2–3), 145–213 (2003).
[185]M. J. Graham and B. G. Lake, Toxicology **254**(3), 184–191 (2008).
[186]M. Martignoni, G. M. M. Groothuis, and R. de Kanter, Expert Opin. Drug Metab. Toxicol. **2**(6), 875–894 (2006).
[187]Y.-C. Toh, T. C. Lim, D. Tai, G. Xiao, D. van Noort, and H. Yu, Lab Chip **9**(14), 2026–2035 (2009).
[188]N. Picollet-D'hahan, A. Zuchowska, I. Lemeunier, and S. Le Gac, Trends Biotechnol. **39**(8), 788–810 (2021).
[189]M. Longmire, P. L. Choyke, and H. Kobayashi, Nanomedicine (London) **3**(5), 703–717 (2008).
[190]A. C. Anselmo and S. Mitragotri, Bioeng. Transl. Med. **4**(3), e10143 (2019).
[191]A. Akhtar, Camb. Q. Healthcare Ethics **24**(4), 407–419 (2015).
[192]S. Qiu, J. Ji, W. Sun, J. Pei, J. He, Y. Li, J. J. Li, and G. Wang, Smart Mater. Med. **2**, 65–73 (2021).
[193]Y. Liu, S. Wang, and Y. Wang, Polymers **8**(11), 402 (2016).
[194]F. Faedmaleki, H. S. F. A, A. Salarian, H. Ahmadi Ashtiani, and H. Rastegar, Iran J. Pharm. Res. **13**(1), 235–242 (2014).
[195]N. Shanks, R. Greek, and J. Greek, Philos., Ethics, Humanities Med. **4**(1), 2 (2009).
[196]J. H. Sung, Y. I. Wang, N. Narasimhan Sriram, M. Jackson, C. Long, J. J. Hickman, and M. L. Shuler, Anal. Chem. **91**(1), 330–351 (2019).
[197]L. Docci, N. Milani, T. Ramp, A. A. Romeo, P. Godoy, D. O. Franyuti, S. Krähenbühl, M. Gertz, A. Galetin, N. Parrott, and S. Fowler, Lab Chip **22**(6), 1187–1205 (2022).
[198]A. Herland, B. M. Maoz, D. Das, M. R. Somayaji, R. Prantil-Baun, R. Novak, M. Cronce, T. Huffstater, S. S. F. Jeanty, M. Ingram, A. Chalkiadaki, D. Benson Chou, S. Marquez, A. Delahanty, S. Jalili-Firoozinezhad, Y. Milton, A. Sontheimer-Phelps, B. Swenor, O. Levy, K. K. Parker, A. Przekwas, and D. E. Ingber, Nat. Biomed. Eng. **4**(4), 421–436 (2020).
[199]C. D. Edington, W. L. K. Chen, E. Geishecker, T. Kassis, L. R. Soenksen, B. M. Bhushan, D. Freake, J. Kirschner, C. Maass, N. Tsamandouras, J. Valdez, C. D. Cook, T. Parent, S. Snyder, J. Yu, E. Suter, M. Shockley, J. Velazquez, J. J. Velazquez, L. Stockdale, J. P. Papps, I. Lee, N. Vann, M. Gamboa, M. E. LaBarge, Z. Zhong, X. Wang, L. A. Boyer, D. A. Lauffenburger, R. L. Carrier, C. Communal, S. R. Tannenbaum, C. L. Stokes, D. J. Hughes, G. Rohatgi, D. L. Trumper, M. Cirit, and L. G. Griffith, Sci. Rep. **8**(1), 4530 (2018).
[200]E. W. Esch, A. Bahinski, and D. Huh, Nat. Rev. Drug Discovery **14**(4), 248–260 (2015).
[201]J. H. Sung, Expert Opin. Drug Metab. Toxicol. **17**(8), 969–986 (2021).
[202]A. Schober, U. Fernekorn, B. Lübbers, J. Hampl, F. Weise, G. Schlingloff, M. Gebinoga, M. Worgull, M. Schneider, C. Augspurger, C. Hildmann, M. Kittler, and M. Donahue, Mater. Werkst. **42**(2), 139–146 (2011).
[203]Y. Zhang, N. Yang, L. Xie, F. Shu, Q. Shi, and N. Shaheen, Micromachines **11**(12), 1–11 (2020).
[204]G. A. Clarke, B. X. Hartse, A. E. Niaraki Asli, M. Taghavimehr, N. Hashemi, M. Abbasi Shirsavar, R. Montazami, N. Alimoradi, V. Nasirian, L. J. Ouedraogo, and N. N. Hashemi, Sensors (Basel) **21**(4), 1367 (2021).
[205]S. Fuchs, S. Johansson, AØ Tjell, G. Werr, T. Mayr, and M. Tenje, ACS Biomater. Sci. Eng. **7**(7), 2926–2948 (2021).
[206]Y. S. Zhang, J. Aleman, S. R. Shin, T. Kilic, D. Kim, S. A. Mousavi Shaegh, S. Massa, R. Riahi, S. Chae, N. Hu, H. Avci, W. Zhang, A. Silvestri, A. Sanati Nezhad, A. Manbohi, F. De Ferrari, A. Polini, G. Calzone, N. Shaikh, P. Alerasool, E. Budina, J. Kang, N. Bhise, J. Ribas, A. Pourmand, A. Skardal, T. Shupe, C. E. Bishop, M. R. Dokmeci, A. Atala, and A. Khademhosseini, Proc. Natl. Acad. Sci. U. S. A. **114**(12), E2293–E2302 (2017).
[207]J. Aleman, T. Kilic, L. S. Mille, S. R. Shin, and Y. S. Zhang, Nat. Protoc. **16**(5), 2564–2593 (2021).
[208]A. Weltin, S. Hammer, F. Noor, Y. Kaminski, J. Kieninger, and G. A. Urban, Biosens. Bioelectron. **87**, 941–948 (2017).
[209]S. R. Shin, T. Kilic, Y. S. Zhang, H. Avci, N. Hu, D. Kim, C. Branco, J. Aleman, S. Massa, A. Silvestri, J. Kang, A. Desalvo, M. A. Hussaini, S. K. Chae, A. Polini, N. Bhise, M. A. Hussain, H. Lee, M. R. Dokmeci, and A. Khademhosseini, Adv. Sci. (Weinh) **4**(5), 1600522 (2017).
[210]K. Jungermann and N. Katz, Physiol. Rev. **69**(3), 708–764 (1989).

[211]L. A. Low, C. Mummery, B. R. Berridge, C. P. Austin, and D. A. Tagle, Nat. Rev. Drug Discovery **20**(5), 345–361 (2021).
[212]N. Franzen, W. H. van Harten, V. P. Retèl, P. Loskill, J. van den Eijnden-van Raaij, and M. IJzerman, Drug Discovery Today **24**(9), 1720–1724 (2019).
[213]U. Marx, T. Akabane, T. B. Andersson, E. Baker, M. Beilmann, S. Beken, S. Brendler-Schwaab, M. Cirit, R. David, E. M. Dehne, I. Durieux, L. Ewart, S. C. Fitzpatrick, O. Frey, F. Fuchs, L. G. Griffith, G. A. Hamilton, T. Hartung, J. Hoeng, H. Hogberg, D. J. Hughes, D. E. Ingber, A. Iskandar, T. Kanamori, H. Kojima, J. Kuehnl, M. Leist, B. Li, P. Loskill, D. L. Mendrick, T. Neumann, G. Pallocca, I. Rusyn, L. Smirnova, T. Steger-Hartmann, D. A. Tagle, A. Tonevitsky, S. Tsyb, M. Trapecar, B. Van de Water, J. Van den Eijnden-van Raaij, P. Vulto, K. Watanabe, A. Wolf, X. Zhou, and A. Roth, Altex **37**(3), 365–394 (2020).
[214]P. L. Candarlioglu, G. Dal Negro, D. Hughes, F. Balkwill, K. Harris, H. Screen, H. Morgan, R. David, S. Beken, O. Guenat, W. Rowan, and A. Amour, Biochem. Soc. Trans. **50**(2), 665–673 (2022).
[215]S. Ya, W. Ding, S. Li, K. Du, Y. Zhang, C. Li, J. Liu, F. Li, P. Li, T. Luo, L. He, A. Xu, D. Gao, and B. Qiu, ACS Appl. Mater. Interfaces **13**(28), 32640–32652 (2021).
[216]J. T. C. Lim, L. G. Kwang, N. C. W. Ho, C. C. M. Toh, N. S. H. Too, L. Hooi, T. Benoukraf, P. K.-H. Chow, Y. Y. Dan, E. K.-H. Chow, T. B. Toh, and E. L. S. Fong, Biomaterials **284**, 121527 (2022).
[217]Y. Zhou, J. X. Shen, and V. M. Lauschke, Front. Pharmacol. **10**, 1093 (2019).
[218]A. J. Wang, A. Allen, M. Sofman, P. Sphabmixay, E. Yildiz, and L. G. Griffith, Adv. NanoBiomed. Res. **2**(1), 2100049 (2022).
[219]G. K. Michalopoulos, J. Cell. Physiol. **213**, 286–300 (2007).
[220]P. Ferenci, Gastroenterol. Rep. **5**(2), 138–147 (2017).
[221]G. K. Michalopoulos and B. Bhushan, *Nature Reviews Gastroenterology and Hepatology* (Nature Research, 2021), pp. 40–55.
[222]S. Yang, Z. Chen, Y. Cheng, T. Liu, L. Yin, Y. Pu, and G. Liang, Environ. Pollut. **268**, 115861 (2021).
[223]A. Kumaran, R. Vashishth, S. Singh, S. U, A. James, and P. Velayudhaperumal Chellam, Microchem. J. **178**, 107420 (2022).
[224]C. Oleaga, A. Lavado, A. Riu, S. Rothemund, C. A. Carmona-Moran, K. Persaud, A. Yurko, J. Lear, N. S. Narasimhan, C. J. Long, F. Sommerhage, L. R. Bridges, Y. Cai, C. Martin, M. T. Schnepper, A. Goswami, R. Note, J. Langer, S. Teissier, J. Cotovio, and J. J. Hickman, Adv. Funct. Mater. **29**(8), 1970049 (2019).
[225]E. Ferrari, C. Palma, S. Vesentini, P. Occhetta, and M. Rasponi, Biosensors (Basel) **10**(9), 110 (2020).
[226]M. Rothbauer and P. Ertl, Adv. Biochem. Eng. Biotechnol. **179**, 343–354 (2022).
[227]Y. Zhu, K. Mandal, A. L. Hernandez, S. Kawakita, W. Huang, P. Bandaru, S. Ahadian, H.-J. Kim, V. Jucaud, M. R. Dokmeci, and A. Khademhosseini, Curr. Opin. Biomed. Eng. **19**, 100309 (2021).
[228]U. Marx, H. Walles, S. Hoffmann, G. Lindner, R. Horland, F. Sonntag, U. Klotzbach, D. Sakharov, A. Tonevitsky, and R. Lauster, Altern. Lab Anim. **40**(5), 235–257 (2012).
[229]E. M. Jacob, A. Borah, and D. Sakthi Kumar, in *Microfluidics and Multi Organs on Chip*, edited by P. V. Mohanan (Springer Nature Singapore, Singapore, 2022), pp. 261–288.
[230]J.-w. Jeon, S. H. Lee, D. Kim, and J. H. Sung, Biotechnol. Prog. **37**(3), e3121 (2021).
[231]J. Kühnl, T. P. Tao, K. Brandmair, S. Gerlach, T. Rings, U. Müller-Vieira, J. Przibilla, C. Genies, C. Jaques-Jamin, A. Schepky, U. Marx, N. J. Hewitt, and I. Maschmeyer, Toxicology **448**, 152637 (2021).
[232]I. Wagner, E.-M. Materne, S. Brincker, U. Süßbier, C. Frädrich, M. Busek, F. Sonntag, D. A. Sakharov, E. V. Trushkin, A. G. Tonevitsky, R. Lauster, and U. Marx, Lab Chip **13**(18), 3538–3547 (2013).
[233]K. Shik Mun, K. Arora, Y. Huang, F. Yang, S. Yarlagadda, Y. Ramananda, M. Abu-El-Haija, J. J. Palermo, B. N. Appakalai, J. D. Nathan, and A. P. Naren, Nat. Commun. **10**(1), 3124 (2019).
[234]A. Essaouiba, T. Okitsu, R. Kinoshita, R. Jellali, M. Shinohara, M. Danoy, C. Legallais, Y. Sakai, and E. Leclerc, Biochem. Eng. J. **164**, 107783 (2020).
[235]S.-H. Hwang, S. Lee, J. Y. Park, J. S. Jeon, Y.-J. Cho, and S. Kim, Micromachines **12**(2), 215 (2021).
[236]M. S. Benedetti, R. Whomsley, I. Poggesi, W. Cawello, F.-X. Mathy, M.-L. Delporte, P. Papeleu, and J.-B. Watelet, Drug Metab. Rev. **41**(3), 344–390 (2009).
[237]S. Ishida, Drug Metab. Pharmacokinet. **33**(1), 49–54 (2018).
[238]J. H. Sung and M. L. Shuler, Lab Chip **9**(10), 1385–1394 (2009).
[239]L. Ewart, A. Apostolou, S. A. Briggs, C. V. Carman, J. T. Chaff, A. R. Heng, S. Jadalannagari, J. Janardhanan, K.-J. Jang, S. R. Joshipura, M. M. Kadam, M. Kanellias, V. J. Kujala, G. Kulkarni, C. Y. Le, C. Lucchesi, D. V. Manatakis, K. K. Maniar, M. E. Quinn, J. S. Ravan, A. C. Rizos, J. F. K. Sauld, J. D. Sliz, W. Tien-Street, D. R. Trinidad, J. Velez, M. Wendell, O. Irrechukwu, P. K. Mahalingaiah, D. E. Ingber, J. W. Scannell, and D. Levner, "Qualifying a human liver-chip for predictive toxicology: Performance assessment and economic implications," bioRxiv (2022).
[240]F. Pisapia, W. Balachandran, and M. Rasekh, Appl. Sci. **12**(8), 3829 (2022).
[241]P. D. Menezes, N. Gadegaard, R. M. Natal Jorge, and S. I. S. Pinto, Int. J. Numer. Methods Biomed. Eng. **37**(5), e3445 (2021).
[242]J. Wang, V. G. Rodgers, P. Brisk, and W. H. Grover, PLoS One **12**(12), e0189429 (2017).
[243]Z. Li, J. Hui, P. Yang, and H. Mao, Biosensors **12**(6), 370 (2022).
[244]Z. Ballard, C. Brown, A. M. Madni, and A. Ozcan, Nat. Mach. Intell. **3**(7), 556–565 (2021).
[245]Y. Mahdi and K. Daoud, J. Dispersion Sci. Technol. **38**(10), 1501–1508 (2017).
[246]D. Stoecklein, K. G. Lore, M. Davies, S. Sarkar, and B. Ganapathysubramanian, Sci. Rep. **7**(1), 46368 (2017).
[247]S. H. Hong, H. Yang, and Y. Wang, Microfluid. Nanofluid. **24**(6), 44 (2020).
[248]M. C. Comes, P. Casti, A. Mencattini, D. Di Giuseppe, F. Mermet-Meillon, A. De Ninno, M. C. Parrini, L. Businaro, C. Di Natale, and E. Martinelli, Sci. Rep. **9**(1), 6789 (2019).
[249]S. Parlato, A. De Ninno, R. Molfetta, E. Toschi, D. Salerno, A. Mencattini, G. Romagnoli, A. Fragale, L. Roccazzello, M. Buoncervello, I. Canini, E. Bentivegna, M. Falchi, F. R. Bertani, A. Gerardino, E. Martinelli, C. Natale, R. Paolini, L. Businaro, and L. Gabriele, Sci. Rep. **7**(1), 1093 (2017).
[250]M. C. Comes, J. Filippi, A. Mencattini, P. Casti, G. Cerrato, A. Sauvat, E. Vacchelli, A. De Ninno, D. Di Giuseppe, M. D'Orazio, F. Mattei, G. Schiavoni, L. Businaro, C. Di Natale, G. Kroemer, and E. Martinelli, Neural Comput. Appl. **33**(8), 3671–3689 (2021).
[251]A. Özkan, D. Stolley, E. N. Cressman, M. McMillin, S. DeMorrow, T. E. Yankeelov, and M. N. Rylander, "The influence of chronic liver diseases on hepatic vasculature: A liver-on-a-chip review," Micromachines **11**(5), 487 (2020).